RRA-T91
NRDL TRC-69-5
15 January 1969

RRA RADIATION RESEARCH ASSOCIATES
Fort Worth, Texas

MONTE CARLO STUDY OF INTERIOR PARTITION EFFECTS ON FALLOUT SHIELDING

Final Report
Contract No. N0022868C1770
(OCD Work Unit No. 1112H)

66

RRA-T91
NRDL TRC-69-5
15 January 1969

MONTE CARLO STUDY OF INTERIOR PARTITION EFFECTS ON FALLOUT SHIELDING

by

J. H. Price and R. L. French

for

Office of Civil Defense
Office of the Secretary of the Army
Washington, D. C. 20310

through the
U.S. Naval Radiological Defense Laboratory
San Francisco, California 94135

OCD Review Notice:

This report has been reviewed in the Office of Civil Defense and approved for publication. Approval does not signify that the contents necessarily reflect the views and policies of the Office of Civil Defense.

Final Report
Contract No. N0022868C1770
(OCD Work Unit No. 1112H)

RADIATION RESEARCH ASSOCIATES, INC.
3550 Hulen Street
Fort Worth, Texas 76107

SUMMARY

Protection factors were calculated for cylindrical concrete barriers with an interior partition using Monte Carlo procedures. The results were compared with protection factors calculated using the Engineering Method, in order to evaluate the ability of the Engineering Method to predict protection factors for cylindrical barriers with interior partitions. The Monte Carlo results were also analyzed to give a better understanding of the effects of the interior partition and to aid in further development of the Engineering Method.

The cylindrical barriers were of concrete and were infinite in height. The radius of the external barrier was 10.0 ft, and the interior partition radii were 2.5, 5.0, and 10.0 ft. The barrier thicknesses were 20, 40, and 80 psf (lbs/ft^2), and the interior partition thicknesses were 20 and 40 psf. The source was an infinite plane ^{60}Co source, assumed to represent fallout.

The results from previous Monte Carlo protection factor calculations for 20-, 40-, and 80-psf cylindrical barriers without interior partitions were used in the comparisons to present barriers with interior partitions of zero thickness. The barrier configuration and source were the same as those used in the protection factor calculations with interior partitions. The previous results were also used to represent barriers with a pseudo partition at a radius of 10.0 ft.

The flux energy and exposure rate angle distributions were also calculated at a height of 3 ft inside the barriers with the interior partitions. These data were obtained for each of 4 components defined by the mode of propagation of the gamma rays through the barriers:

Exterior Barrier Propagation	Interior Partition Propagation	Designation
Direct Beam	Direct Beam	EDB-IDB
Scattered	Direct Beam	EBS-IDB
Direct Beam	Scattered	EDB-IBS
Scattered	Scattered	EBS-IBS

The components were summed to give the total.

The barrier-scattered components (i.e., EBS-IDB, EDB-IBS, and EBS-IBS) were calculated by Monte Carlo. The EDB-IDB component was calculated by analytic procedures.

Using the Engineering Method, protection factors were calculated for the same configurations described above. The Engineering Method results were calculated in terms of a direct-beam and barrier-scattered exposure rate inside the barriers. This allowed comparison with Monte Carlo results on a component basis.

Inspection of the Monte Carlo results indicated that, as the locations of the interior partitions were varied, the Monte Carlo protection factors showed no consistent dependence upon the location of the partition. Overall, the protection factor increased an average of 8.0 percent as the radius increased from 2.5 to 10.0 ft. The location becomes more important as the barrier or partition thickness is increased. Over the range of radii and barrier thicknesses used here, it was concluded that the location of the partition is unimportant. The neglect of the location of the partition in the Engineering Method is consistent with this conclusion.

The 40-psf partition increased the protection factors of the various barrier configurations by factors ranging from 1.97 to 2.47. The increases were all the same within 26 percent. This indicates that some average barrier reduction factor which is a function only of the partition thickness could be used in calculating the effect of the partition. This is consistent with the Engineering Method in that the partition barrier reduction factor is assumed to be a function only of the partition thickness.

The Monte Carlo and Engineering Method protection factors were compared. The average difference was 7.7 percent, with the largest difference approximately 22 percent. The Engineering Method results were generally higher. This same trend was also noted in previous experimental studies.

Average barrier reduction factors for the interior partitions were calculated from the Monte Carlo data for each partition thickness. The results were found to be larger than similar Engineering Method data by 0, 9, and 25 percent for 0-, 20-, and 40-psf partitions.

The new barrier reduction factors were used in additional Engineering Method calculations. The results were compared with Monte Carlo protection factors and found to agree much better than did the original Engineering Method data. Also, the new results were on the conservative side of the Monte Carlo protection factors.

It was concluded that the assumptions used in the Engineering Method for predicting the effects of interior partitions in fallout shielding are reasonable. However, new barrier reduction factors should be calculated for the partitions. At present, the same barrier reduction factor curves are used for both the exterior barriers and the partitions.

Before incorporating new partition barrier reduction factors, it would be necessary to extend the range of the barrier and partition thicknesses and locations considered in this study to determine the exact range for which the assumptions used in the Engineering Method are valid. It would also be necessary to determine the exact dependence of $B_i'(X_i)$ on the geometric shape of the partition. It should be noted that these conclusions are based on a cylindrical geometry and may not apply to other geometries.

RRA-T91
NRDL TRC-69-5
15 January 1969

MONTE CARLO STUDY OF INTERIOR PARTITION EFFECTS ON FALLOUT SHIELDING

by

J. H. Price and R. L. French

for

Office of Civil Defense
Office of the Secretary of the Army
Washington, D. C. 20310

through the
U.S. Naval Radiological Defense Laboratory
San Francisco, California 94135

OCD Review Notice:

This report has been reviewed in the Office of Civil Defense and approved for publication. Approval does not signify that the contents necessarily reflect the views and policies of the Office of Civil Defense.

Final Report
Contract No. N0022868C1770
(OCD Work Unit No. 1112H)

RADIATION RESEARCH ASSOCIATES, INC.
3550 Hulen Street
Fort Worth, Texas 76107

ABSTRACT

Protection factors were calculated by Monte Carlo for cylindrical barriers with a concentric interior partition. The barrier thicknesses were 20, 40, and 80 psf and the partition thicknesses were 20 and 40 psf. The radius of the barrier was 10.0 ft and the interior partition had radii of 2.5, 5.0, and 10.0 ft. The cylindrical concrete barriers were infinite in height. The source was an infinite plane ^{60}Co source which was assumed to represent fallout. The Engineering Method was also used to calculate protection factors for the cylindrical barriers, and the results were compared with the Monte Carlo data.

The Monte Carlo protection factors showed no consistent dependence upon the radius of the partition. The 40-psf partition was found to increase the protection factors of the barriers by as much as a factor of 2.47. The increases in the protection factors due to the 40-psf partition were all the same within 26 percent for the different partition radii and barrier thicknesses. The Monte Carlo and Engineering Method protection factors had an average difference of 7.7 percent with the largest difference being 22 percent. The Engineering Method results were consistently higher. Interior partition reduction factors were calculated from the Monte Carlo data. These factors were found to be as much as 25 percent higher than similar Engineering Method reduction factors. Use of these reduction factors in the Engineering Method gave protection factors which agreed much better with the Monte Carlo protection factors.

TABLE OF CONTENTS

		Page
	ABSTRACT	ii
	LIST OF FIGURES	iv
	LIST OF TABLES	v
	SUMMARY	vi
I.	INTRODUCTION	1
II.	MONTE CARLO CALCULATIONS	4
	2.1 Free-Field Radiation Calculations	4
	2.2 Pseudo Source Description	5
	2.3 Barrier Penetration Calculations	7
	2.3.1 Barrier-Scattered Components	8
	2.3.2 Direct-Beam Component	11
III.	ENGINEERING METHOD CALCULATIONS	12
	3.1 Description of Method	12
	3.2 Parameter Data and Results	14
IV.	RESULTS AND ANALYSIS	17
	4.1 Analysis of Components	19
	4.2 Effect on Protection Factor of Partition Location	21
	4.3 Effect on Protection Factor of Barrier and Partition Thickness	25
	4.4 Comparisons of Monte Carlo, Experimental, and Engineering Method Protection Factors	27
V.	CONCLUSIONS	34
	REFERENCES	36
	APPENDIX A: Gamma-Ray Energy and Angle Distributions Inside Concentric Cylindrical Barriers Exposed to Infinite Plane ^{60}Co Source	37
	APPENDIX B: GRAS1 Monte Carlo Procedure	48

LIST OF FIGURES

Figure		Page
1.	Geometry for Interior Partition Study	2
2.	Comparison of the Angle Distribution of the Barrier-Scattered Exposure Rate Inside an 80-psf Barrier	10
3.	Angle Distribution of the Scattered Exposure Rate Inside a 20-psf Barrier with and without 40-psf Partition	22
4.	Scattered Flux Energy Distribution Inside a 40-psf Barrier with and without 40-psf Partition	23
5.	Protection Factor vs. Partition Radius for Concentric Cylindrical Barriers	24
6.	Protection Factor vs. Exterior Barrier Thickness for Concentric Cylindrical Barriers	26
7.	Protection Factor vs. Partition Thickness for Concentric Cylindrical Barriers (Partition Radius = 2.5 ft)	29
8.	Protection Factor vs. Partition Thickness for Concentric Cylindrical Barriers (Partition Radius = 5.0 ft)	30
9.	Protection Factor vs. Partition Thickness for Concentric Cylindrical Barriers (Partition Radius = 10.0 ft)	31

LIST OF TABLES

Table		Page
I.	Energy and Angle Distribution of the Free-Field Radiation 3 ft above Infinite Plane ^{60}Co Source	6
II.	Numerical Value of Parameters for Engineering Method Calculations	15
III.	Engineering Method Data for Concentric Cylindrical Barriers Exposed to Infinite Plane ^{60}Co Source	16
IV.	Penetration Data for Concentric Cylindrical Barriers Exposed to Infinite Plane ^{60}Co Source	18
V.	Penetration Data for Simple Cylindrical Barriers Exposed to Infinite Plane ^{60}Co Source	19

SUMMARY

Protection factors were calculated for cylindrical concrete barriers with an interior partition using Monte Carlo procedures. The results were compared with protection factors calculated using the Engineering Method, in order to evaluate the ability of the Engineering Method to predict protection factors for cylindrical barriers with interior partitions. The Monte Carlo results were also analyzed to give a better understanding of the effects of the interior partition and to aid in further development of the Engineering Method.

The cylindrical barriers were of concrete and were infinite in height. The radius of the external barrier was 10.0 ft, and the interior partition radii were 2.5, 5.0, and 10.0 ft. The barrier thicknesses were 20, 40, and 80 psf (lbs/ft^2), and the interior partition thicknesses were 20 and 40 psf. The source was an infinite plane ^{60}Co source, assumed to represent fallout.

The results from previous Monte Carlo protection factor calculations for 20-, 40-, and 80-psf cylindrical barriers without interior partitions were used in the comparisons to present barriers with interior partitions of zero thickness. The barrier configuration and source were the same as those used in the protection factor calculations with interior partitions. The previous results were also used to represent barriers with a pseudo partition at a radius of 10.0 ft.

The flux energy and exposure rate angle distributions were also calculated at a height of 3 ft inside the barriers with the interior partitions. These data were obtained for each of 4 components defined by the mode of propagation of the gamma rays through the barriers:

Exterior Barrier Propagation	Interior Partition Propagation	Designation
Direct Beam	Direct Beam	EDB-IDB
Scattered	Direct Beam	EBS-IDB
Direct Beam	Scattered	EDB-IBS
Scattered	Scattered	EBS-IBS

The components were summed to give the total.

The barrier-scattered components (i.e., EBS-IDB, EDB-IBS, and EBS-IBS) were calculated by Monte Carlo. The EDB-IDB component was calculated by analytic procedures.

Using the Engineering Method, protection factors were calculated for the same configurations described above. The Engineering Method results were calculated in terms of a direct-beam and barrier-scattered exposure rate inside the barriers. This allowed comparison with Monte Carlo results on a component basis.

Inspection of the Monte Carlo results indicated that, as the locations of the interior partitions were varied, the Monte Carlo protection factors showed no consistent dependence upon the location of the partition. Overall, the protection factor increased an average of 8.0 percent as the radius increased from 2.5 to 10.0 ft. The location becomes more important as the barrier or partition thickness is increased. Over the range of radii and barrier thicknesses used here, it was concluded that the location of the partition is unimportant. The neglect of the location of the partition in the Engineering Method is consistent with this conclusion.

The 40-psf partition increased the protection factors of the various barrier configurations by factors ranging from 1.97 to 2.47. The increases were all the same within 26 percent. This indicates that some average barrier reduction factor which is a function only of the partition thickness could be used in calculating the effect of the partition. This is consistent with the Engineering Method in that the partition barrier reduction factor is assumed to be a function only of the partition thickness.

The Monte Carlo and Engineering Method protection factors were compared. The average difference was 7.7 percent, with the largest difference approximately 22 percent. The Engineering Method results were generally higher. This same trend was also noted in previous experimental studies.

Average barrier reduction factors for the interior partitions were calculated from the Monte Carlo data for each partition thickness. The results were found to be larger than similar Engineering Method data by 0, 9, and 25 percent for 0-, 20-, and 40-psf partitions.

The new barrier reduction factors were used in additional Engineering Method calculations. The results were compared with Monte Carlo protection factors and found to agree much better than did the original Engineering Method data. Also, the new results were on the conservative side of the Monte Carlo protection factors.

It was concluded that the assumptions used in the Engineering Method for predicting the effects of interior partitions in fallout shielding are reasonable. However, new barrier reduction factors should be calculated for the partitions. At present, the same barrier reduction factor curves are used for both the exterior barriers and the partitions.

Before incorporating new partition barrier reduction factors, it would be necessary to extend the range of the barrier and partition thicknesses and locations considered in this study to determine the exact range for which the assumptions used in the Engineering Method are valid. It would also be necessary to determine the exact dependence of $B_i'(X_i)$ on the geometric shape of the partition. It should be noted that these conclusions are based on a cylindrical geometry and may not apply to other geometries.

I. INTRODUCTION

Over the past several years, a small number of experiments have been performed to determine the protection afforded by various structures with interior partitions when exposed to a simulated fallout field.[1,2,3] The results, expressed as protection factors, were compared with similar results calculated with the well known "Engineering Method".[4] The Engineering Method, which was developed by N. FitzSimons and C. Eisenhauer from the moments-method data reported in NBS Monograph 42,[5] was found to be in reasonable agreement with the experiments, although the Engineering Method protection factors were generally high. However, it was recently suggested that the Engineering Method for treating interior partitions is in error,[6] and that its success is due to off-setting errors in the method.

The objective of the present study is to use Monte Carlo methods to evaluate and possibly develop further the Engineering Method treatment of the interior partition problem. In particular, Monte Carlo calculations should yield sufficiently detailed information to determine whether the assumptions and/or data used in the Engineering Method produce off-setting errors.

The geometry used for the study consists of 2 concentric right circular cylinders located normal to the ground as shown in Figure 1. The barriers are assumed to be infinite in height; therefore, no roof contributions are considered. The cylindrical barrier geometry was used to be consistent with that used in previous Monte Carlo studies.[7,8] Many of the parameters used in this study, such as barrier thickness, barrier radius, the energy and angle groups for both the source and the results, and the source term, were the same as those used previously.

This allowed the results from the previous studies to be used herein for barriers with no partitions. The results were also used for barriers with pseudo partitions. For example, the results for the 80-psf barrier were used to represent a 40-psf barrier with a 40-psf partition whose outer radius was equal to the inner radius of the exterior barrier.

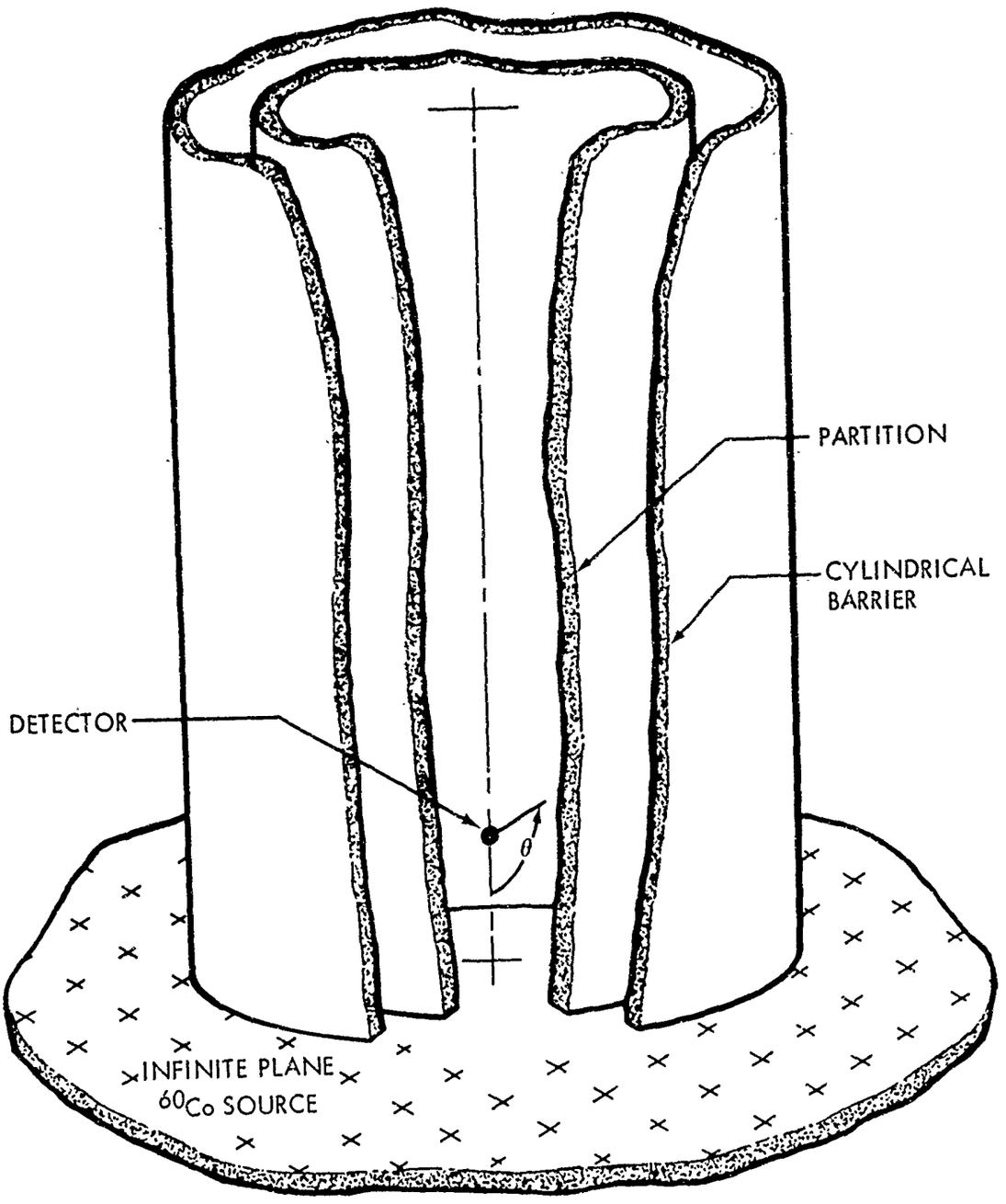

Fig. 1. Geometry for Interior Partition Study

The barriers and partitions are composed of ordinary concrete. The source is assumed to be an infinite plane of ^{60}Co(~1.25 MeV) located on the ground surface. The detector was located 3 ft above the ground on the vertical axis of the barriers.

The parameters that were varied were the exterior barrier thickness, the interior partition thickness, and the radius of the partition. The values calculated for each configuration were the flux energy distribution and the exposure rate polar angle distribution. The total flux and exposure rate were also determined. These data were calculated for each of 4 components representing different modes of propagation of the gamma rays through the barrier and partition.

From these Monte Carlo data, protection factors were calculated for each barrier configuration. These factors were compared with measured protection factors and with protection factors calculated using the Engineering Method.

The Monte Carlo calculations are described in Section II. A description of the source term and its application to the problem are included. The Engineering Method for interior partition calculations is described in Section III. Included are the numerical values of the various parameters used in the calculations.

Section IV presents the Monte Carlo results in integral form, gives a detailed analysis of the Monte Carlo results, and compares them with experimental and Engineering Method results. The detailed energy and angle distributions are given in Appendix A. Appendix B describes modifications made to the GRASS Monte Carlo procedure[9] to make it applicable to the interior partition problem and to improve its efficiency.

II. MONTE CARLO CALCULATIONS

To determine the protection factor of a barrier, it is necessary to calculate 1) the free-field exposure rate and 2) the exposure rate inside the barrier. The free-field flux and exposure rate 3 ft above an infinite smooth plane of ^{60}Co were calculated in a previous study.[7] The results of those free-field calculations were used in this study.

The free-field flux was used to develop a pseudo source. This source was used in the barrier penetration calculations made to determine the exposure rate inside the barriers. The following sub-section gives a brief description of the free-field calculations described in detail in Reference 7. The pseudo source is described in Section 2.2. Section 2.3 describes the barrier penetration calculations and the protection factor calculations.

2.1 Free-Field Radiation Calculations

The free-field calculations consisted of computing the flux energy and angle distributions of both the uncollided and the air- and ground-scattered gamma rays 3 ft above an infinite plane ^{60}Co (~1.25 MeV) source. The COHORT Monte Carlo procedure[10] was used for the scattered gamma-ray calculations. The angle distribution of the uncollided gamma rays was computed analytically using the RRA-65A procedure.[8]

The polar angle distribution of the two components (i.e., uncollided and scattered flux) were computed in terms of the absolute number flux in each of 18 ten-degree intervals (i.e., 0-10, 10-20, ...170-180 degrees) on polar angle. The polar angle is measured with respect to the normal to the source plane. The results were integrated over azimuthal angle. The scattered flux was sorted into 8 energy groups defined by the limits: 0.04-0.06, 0.06-0.10, 0.10-0.18, 0.18-0.30, 0.30-0.50, 0.50-0.75, 0.75-1.00, and 1.00-1.25 MeV. The free-field flux was converted to exposure rate using the conversion factors from Reference 11. A source strength of 1 photon/cm^2-sec was assumed for the calculations.

The results of these calculations are given in Table I and consist of: 1) the flux energy and angle distribution, 2) the total flux and exposure rate angle distribution, 3) the total flux energy distribution, and 4) the total free-field flux and exposure rate.

2.2 Pseudo Source Description

For the barrier penetration calculations, it was assumed that the energy and angle distribution of the free-field flux is not disturbed by the barrier. It has been shown that the exposure rate inside a barrier is increased very little by gamma rays incident on the barrier more than a few feet above or below the detector height.[7] Thus, it was assumed that the flux incident at any point on the barrier could be described by the distribution of the free-field flux at the 3-ft detector height.

The energy and angle distribution of the free-field flux was used to generate a pseudo source. This source was located on the outside surface of the exterior barrier and extended to a height of 23 ft. The height of the barrier was 46 ft. The pseudo source is represented in the barrier penetration calculations in the form of probability distribution tables which are defined in terms of the energy and angle intervals given above for the free-field results. The source is described by a polar angle distribution for each energy interval and an energy probability distribution. Due to the azimuthal symmetry of the infinite plane source, the pseudo source has a cosine distribution on azimuthal angle.

These probability distributions were used in the Monte Carlo calculations to select the initial energy and direction of each gamma ray started from the pseudo source. The energy and direction of the gamma rays were assumed to be uniformly distributed within each angle and energy interval, except the 1.0-1.25 MeV energy group. Inspection of Table I indicates that approximately 97% of the flux in this group is due to uncollided gamma rays that have an energy of 1.25 MeV. For this reason, approximately 97% of the gamma rays within this energy group were given an initial energy of 1.25 MeV. The remainder were evenly distributed over the energy interval.

Table I. Energy and Angle Distribution of the Free-Field Radiation 3 ft Above Infinite Plane ^{60}Co Source

(photons/cm^2-sec per photon/cm^2-sec)

Polar Angle (deg)	Energy (MeV)									Total Flux	Exposure Rate (R/hr)
	0.06	0.10	0.18	0.30	0.50	0.75	1.00	1.25[a]	1.25[b]		
10	0.000-0	0.000-0	0.000-0	1.930-3	3.930-3	0.000-0	0.000-0	0.000-0	7.603-3	1.346-2	2.164-8
20	2.960-6[c]	1.340-3	9.170-3	1.130-2	2.810-2	0.000-0	0.000-0	0.000-0	2.328-2	7.319-2	8.445-8
30	4.030-3	5.530-3	3.300-3	4.340-3	4.010-3	0.000-0	0.000-0	0.000-0	4.051-2	6.171-2	1.007-7
40	7.440-4	3.080-2	1.120-2	4.010-2	1.230-2	0.000-0	0.000-0	0.000-0	6.083-2	1.559-1	1.760-7
50	1.780-6	1.400-4	1.791-2	1.660-2	7.650-3	1.010-2	0.000-0	0.000-0	8.687-2	1.392-1	2.312-7
60	5.230-5	2.000-4	1.210-2	1.390-2	1.310-2	0.000-0	1.150-2	0.000-0	1.241-1	1.749-1	3.254-7
70	2.302-3	5.440-3	1.737-2	1.840-2	1.140-2	7.320-3	4.340-4	0.000-0	1.868-1	2.494-1	4.631-7
80	3.708-3	2.275-2	1.769-2	4.182-2	1.380-2	1.080-2	1.950-2	3.930-3	3.294-1	4.633-1	8.520-7
90	4.594-3	2.368-2	2.456-2	3.725-2	2.176-2	2.282-2	4.005-2	4.484-2	1.343-0	1.552-0	3.326-6
100	9.815-3	2.717-2	3.145-2	4.307-2	2.130-2	2.653-2	2.645-2	2.562-2	0.000-0	2.114-1	1.833-7
110	1.495-2	1.529-2	1.926-2	2.126-2	1.163-2	7.199-3	1.165-2	0.000-0	0.000-0	1.012-1	5.772-8
120	1.687-2	3.033-2	1.540-2	3.661-2	8.623-3	9.308-3	0.000-0	0.000-0	0.000-0	1.171-1	4.668-8
130	9.270-3	1.465-2	4.729-2	1.978-2	1.378-2	1.487-2	0.000-0	0.000-0	0.000-0	1.196-1	5.461-8
140	1.141-2	1.611-2	1.475-2	1.021-2	1.128-2	8.210-3	0.000-0	0.000-0	0.000-0	7.196-2	3.212-8
150	5.340-3	6.804-3	1.396-2	1.954-2	8.550-3	0.000-0	0.000-0	0.000-0	0.000-0	5.419-2	2.136-8
160	2.739-3	1.469-2	8.939-3	7.394-3	2.518-4	0.000-0	0.000-0	0.000-0	0.000-0	3.401-2	3.314-9
170	1.326-3	5.004-3	3.019-3	2.466-3	1.260-3	0.000-0	0.000-0	0.000-0	0.000-0	1.307-2	3.827-9
180	1.094-3	5.737-4	1.968-3	1.380-3	0.000-0	0.000-0	0.000-0	0.000-0	0.000-0	5.015-3	1.367-9
Total	8.827-2	2.205-1	2.693-1	3.474-1	1.927-1	1.171-1	1.096-1	7.439-2	2.276-0	3.611-0	5.989-6

a - Air- and Ground-Scattered Radiation only.
b - Uncollided Radiation Component.
c - Read 2.960-6 as 2.960×10^{-6}.

2.3 Barrier Penetration Calculations

The quantities calculated in the barrier penetration calculations include: 1) the total flux, 2) the total exposure rate, 3) the flux energy distribution, and 4) the exposure rate polar angle distribution. The flux energy distribution was calculated for eight energy groups and the exposure rate angle distributions for 18 ten-degree polar angle groups. The energy and angle groups are the same as those used for the free-field calculations. Each of these quantities was calculated for a point detector located at a height of 3 ft on the centerline of the concentric cylindrical concrete barriers. The results were integrated over azimuthal angle.

The calculations were made for the 12 possible combinations of the following parameters:

1) Partition thicknesses of 20 and 40 psf
2) Exterior barrier thicknesses of 20, 40, and 80 psf
3) Partition radii of 2.5 and 5.0 ft.

The exterior barrier had an outer radius of 10 ft.

Each of the quantities described above was calculated separately for each of 4 components defined by the mode of gamma-ray propagation through the barriers:

Exterior Barrier Propagation	Partition Propagation	Designation
Direct Beam	Direct Beam	EDB-IDB
Scattered	Direct Beam	EBS-IDB
Direct Beam	Scattered	EDB-IBS
Scattered	Scattered	EBS-IBS

The four components were summed to give the total of each quantity calculated. Knowing the total exposure rate inside each barrier and the free-field exposure rate, the protection factor for each of the barriers may be determined. The protection factor is defined as the free-field exposure rate divided by the exposure rate inside the barrier.

The barrier penetration calculations were performed by separate methods for the barrier-scattered components (i.e., EBS-IDB, EDB-IBS, and EBS-IBS) and the direct-beam component (EDB-IDB). The calculations are described separately below. The results of the penetration calculations and the protection factors are given in Section IV.

2.3.1 Barrier-Scattered Components

The barrier-scattered components were computed using a modified version of the GRASS Monte Carlo procedure.[9] The modifications were made to include: 1) a generalized geometry capable of treating basements as well as interior partitions, 2) the separation of the exposure rate inside the barrier into components that are defined by the mode of propagation of the gamma rays through the barrier, and 3) biasing techniques to improve the statistical accuracy of the EDB-IBS and EBS-IBS components.

The modified version of GRASS is designated GRAS1. A description of the modifications is given in Appendix B and a complete description of GRASS is given in Reference 9. GRAS1 will be briefly described here as it pertains to the interior partition problem.

GRAS1 calculates the barrier-scattered flux energy and exposure rate polar angle distribution at a point inside concentric cylindrical barriers. The gamma-ray source is a pseudo source located on the outside surface of the exterior barrier. This pseudo source is defined by probability distributions obtained from the energy and angle distributions of the incident flux, and by the total number of photons incident upon the barrier. (See Section 2.2.)

Once the initial gamma-ray energy, direction, and spatial position are determined from the proper probability distributions, Monte Carlo techniques are used to trace the path of the gamma ray as it scatters within the defined geometry. Each gamma ray is traced until it reaches a specified minimum energy or weight, has a specified number of collisions, or escapes from the defined geometry. A statistical estimate of the scattered flux reaching a point detector is made from each collision point. The sum of

these estimates divided by the number of gamma rays traced gives an estimate of the scattered flux per photon incident upon the barrier. The total scattered flux is obtained by multiplying this quantity by the number of incident photons.

The flux is recorded for each of the three barrier-scattered components in terms of eight energy groups and the exposure rate polar angle distribution in 18 ten-degree intervals. All results are integrated with respect to azimuthal angle. Also calculated are the total flux and exposure rate.

To determine if GRAS1 was working properly, GRAS1 calculations were made of the energy and angle distributions inside a 40-psf exterior cylindrical barrier with an adjacent 40-psf partition. The results were compared with the results from the previous Monte Carlo calculations for an 80-psf barrier. The total exposure rate was found to agree within 2.5% while the total flux agreed within 1.5%. A comparison of the exposure rate polar angle distribution is shown in Figure 2. The results are seen to agree quite well, but the GRAS1 results (based on only 1000 histories) are not as smooth as the GRASS Monte Carlo data, which are for a much larger number of histories. Similar agreement was found for the flux energy distribution. Comparisons made for barriers having a total thickness of 20 and 40 psf gave similar results. It was concluded that GRAS1 was working properly.

From these comparisons, it was also concluded that the results of the previous study could be used as a basis of comparison in the present study. Any differences found between the results for the barrier with and without partitions are caused by the partition and not by differences in the methods of calculation.

GRAS1 calculations were made in steps of 500 histories per problem to give some indication of the statistical accuracy of the calculations. To get from 16,000 to 18,000 collisions for each configuration, it was necessary to run two, three, and four problems for the 80-, 40-, and 20-psf barrier configurations, respectively. The number of collisions per history decreases as the barrier thickness decreases. The results from like problems were averaged to give the final results. The standard deviation of

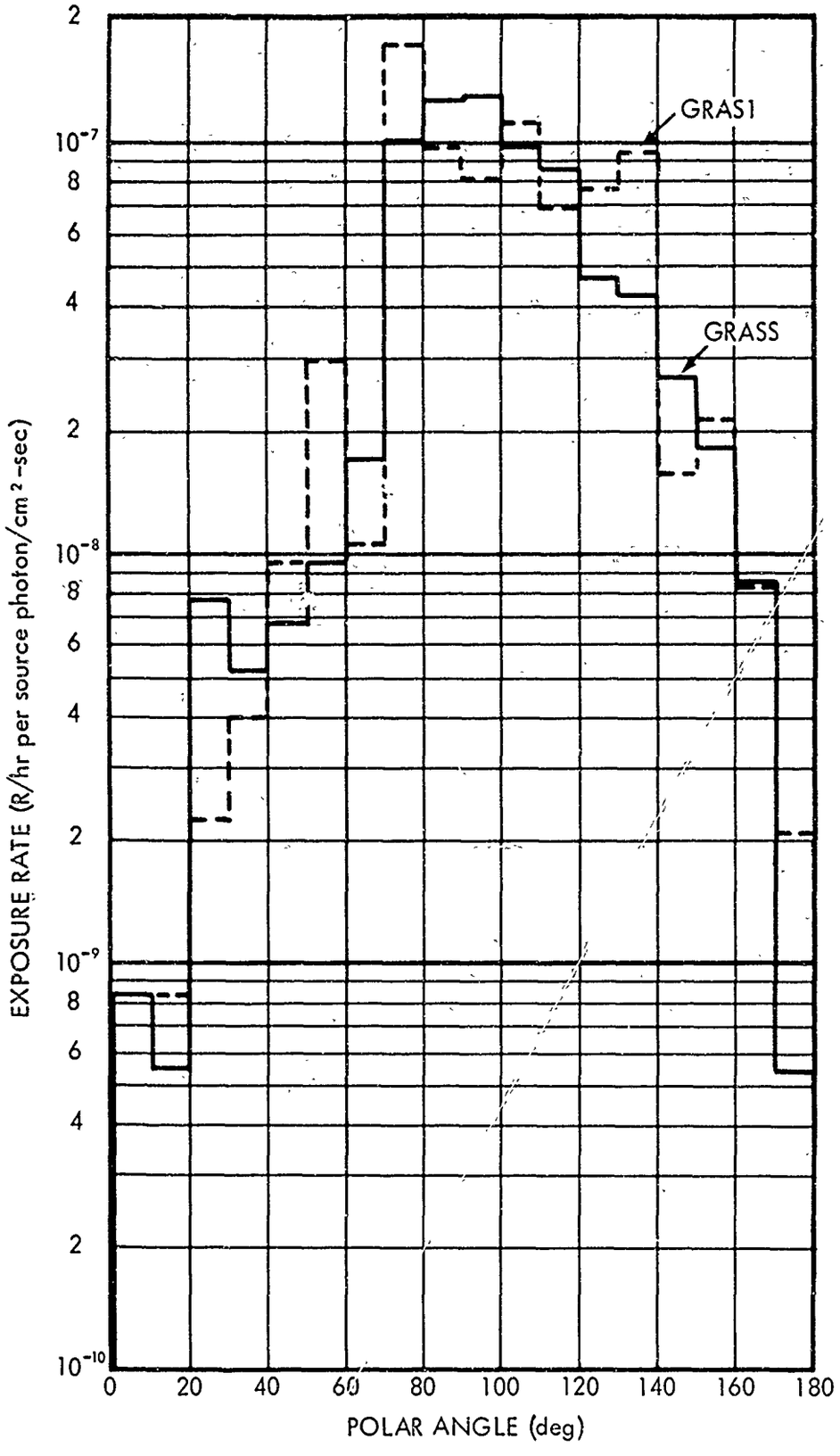

Fig. 2. Comparison of the Angle Distribution of the Barrier-Scattered Exposure Rate Inside an 80-psf Barrier

the total barrier-scattered exposure rate for the 20-psf barriers was found to range from 9 to 20 percent with the average standard deviation being approximately 14 percent.

The accuracy of the results for the 40- and 80-psf barriers should be about the same, because approximately the same number of collisions was used for each configuration.

All cross sections used in the calculations were taken from Reference 12. The exposure rate conversion factors were the same as those used in the free-field radiation calculations.

2.3.2 Direct-Beam Component

The direct-beam component (EDB-IDB) was calculated using existing analytical procedures RRA-65A[8] and RRA-67.[7] The calculations were done in 2 parts which are defined by the mode of propagation of the gamma rays before reaching the barrier: 1) gamma rays incident on the barrier after having at least one collision in the air and/or ground, and 2) gamma rays incident on the barrier before undergoing a collision.

The RRA-67 procedure was used for the first part. This procedure computes attenuation factors for the barrier and partition for each energy and angle group of the air- and ground-scattered free-field flux given in Table I. It multiplies these factors by the corresponding flux values given in the table. The procedure then performs a flux-to-exposure rate conversion and sums over energy and angle to obtain the total exposure rate.

The second part of the EDB-IDB component is one of the most important components of the total exposure rate. It was calculated by the RRA-65A procedure which integrates over the entire infinite plane source and applies exponential attenuation to the flux from each differential source area. The results were then converted to exposure rate and added to the results of part 1 of the calculation to obtain the total direct-beam component.

III. ENGINEERING METHOD CALCULATIONS

The Engineering Method for predicting the protection factor of a structure is described in detail in Reference 4 (OCD-PM-100-1). The brief description given in this section describes the method for handling problems involving interior partitions. No roof contributions are considered. The curves and charts given in OCD-PM-100-1 are based on moments-method data for 1.12-hr fallout given in NBS-42.[5] Corresponding moments-method data for ^{60}Co are given in Appendix B of NBS-42. The necessary curves for ^{60}Co were generated from these data for use in the Engineering Method protection factor calculations. The geometry factors used for ^{60}Co were those calculated by LeDoux from the NBS-42 moments-method data and reported by Kaplan in Reference 2.

Protection factors were calculated using the Engineering Method for each of the barrier configurations described in Section II. The equations used for the calculations are described below. The sources of data and the numerical values of the many parameters required in the calculations are also given.

3.1 Description of Method

The Engineering Method for predicting the protection factor of a cylindrical barrier of infinite height with an interior partition consists of 1) determining a reduction factor assuming no partition, and 2) multiplying this reduction factor by an interior partition barrier reduction factor. The protection factor is the reciprocal of this product.

The Engineering Method assumes that:

1. The protection afforded by the partition is independent of the solid angle subtended by the partition.
2. The partition barrier reduction factor is independent of the shape of the partition.
3. The same barrier reduction factor curves may be used for both the exterior barrier and the partition.

The partition barrier reduction factor is a function only of the partition thickness.

The Engineering Method equation for the reduction factor for a cylindrical barrier with no partition is

$$R_f = B_e(X_e,H)\{[G_d(\omega_\ell) + G_u(\omega_u)][1-S_w(X_e)]\}$$

$$+ B_e(X_e,H)\{[G_s(\omega_\ell) + G_s(\omega_u)][S_w(X_e)][E]\}$$

where $B_e(X_e,H)$ is the barrier reduction factor at a detector height H for a vertical slab of thickness X_e,

$G_d(\omega_\ell)$ is the directional response function for direct radiation,

$G_u(\omega_u)$ is the directional response function for air-scattered radiation,

$G_s(\omega_\ell)$ is the directional response function for barrier-scattered radiation from below the detector plane,

$G_s(\omega_u)$ is the directional response function for barrier-scattered radiation from above the detector plane,

$S_w(X_e)$ is a weighting factor that approximates the fraction of the radiation reaching the detector which is scattered in the barrier,

and E is the shape factor for barrier-scattered radiation ($E = \pi/2$ for a cylinder).[13]

The directional response functions are a function of the solid angle fraction, ω, which is defined as the solid angle subtended by the exterior barrier at the detector, divided by 2π. The subscripts u and ℓ are used to denote the solid angle fractions above and below the detector, respectively. For a cylinder, $\omega = 1.0\text{-cosine}\theta$ where θ is the angle formed between the centerline and a line connecting the top or bottom of the barrier to the detector.

The protection factor for a barrier with a partition is given by the equation

$$P_f = \frac{1.0}{[R_f][B_i(X_i)]}$$

where $B_i(X_i)$ is the barrier reduction factor for a partition of thickness X_i.

Since the weighting factor, $S_w(X_e)$, approximates the fraction of radiation reaching the detector which has been scattered in the barrier,[13] the first term on the right hand side of the reduction factor equation may be interpreted as the direct-beam component and the second term as the barrier-scattered component. To allow direct comparisons with the Monte Carlo results, the Engineering Method results are presented in terms of the direct-beam and barrier-scattered components in addition to the total protection factor.

3.2 Parameter Data and Results

The figures and charts given in OCD-PM-100-1 are based on the moments-method data given in Reference 4 (NBS-42) for 1.12-hr fallout. Corresponding moments-method data for ^{60}Co are given in Appendix B of NBS-42. The necessary curves for ^{60}Co were generated from these data. The moments-method data used to evaluate the parameters in the Engineering Method calculations are:

Parameter	Figure	Reference
B_e, B_i	Fig. B25	Ref. 5
G_d, G_u, G_s	Fig. 2	Ref. 2
S_w	Fig. B23	Ref. 5

It is often very difficult to duplicate protection factor calculations for even a simple structure because of minor differences in reading the numerical value of the various parameters from the curves. Thus, to document fully the calculations reported here, the numerical values of each of the parameters used are given in Table II.

The results of the Engineering Method protection factor calculations are given in Table III. The direct-beam and barrier-scattered components are expressed in units of R/hr per source photon/cm^2-sec. The results are based on a free-field exposure rate of 6.055×10^{-6} R/hr obtained from the moments-method data in NBS Monograph 42.

Table II. Numerical Value of Parameters for Engineering Method Calculations

Parameter	X(psf) 20	40	80	Parameter	ω_u 0.026	ω_ℓ 0.713
B_e	0.625	0.380	0.143	G_s	0.496	0.278
B_i	0.625	0.380	-----	G_u	0.088	-----
S_w	0.327	0.505	0.699	G_d	-----	0.642

Table III. Engineering Method Data for Concentric Cylindrical Barriers Exposed to Infinite Plane ^{60}Co Source

(R/hr per source photon/cm^2-sec)

Radiation Component	Barrier Thickness 20	40	80
	0-psf Interior Partition		
Direct Beam	1.859-6*	8.324-7	1.901-7
Scattered	1.504-6	1.413-6	7.363-7
Total	3.363-6	2.245-6	9.264-7
Protection** Factor	1.800	2.696	6.535
	20-psf Interior Partition		
Direct Beam	1.162-6	5.201-7	1.188-7
Scattered	9.405-7	8.833-7	4.605-7
Total	2.103-6	1.404-6	5.793-7
Protection Factor	2.879	4.314	10.450
	40-psf Interior Partition		
Direct Beam	7.070-7	3.162-7	7.228-8
Scattered	5.719-7	5.369-7	2.800-7
Total	1.279-6	8.531-7	3.523-7
Protection Factor	4.734	7.097	17.190

* Read 1.859-6 as 1.859×10^{-6}.

** $D_o = 6.055 \times 10^{-6}$ (R/hr per source photon/cm^2-sec) based on moments method data from Reference 5.

IV. RESULTS AND ANALYSIS

The results of the Monte Carlo barrier penetration calculations are summarized in Table IV. The exposure rate is given for each of the four components described in Section 2.3. The detector is at a height of 3 ft on the centerline of the concentric cylindrical barriers. The barriers have exterior thicknesses of 20, 40, and 80 psf and partition thicknesses of 20 and 40 psf. The results are given for partition radii of both 2.5 and 5.0 ft. The outer radius of the exterior barrier is 10.0 ft, and the infinite plane ^{60}Co source on the ground surface has a strength of 1 photon/cm^2-sec.

Also given in Table IV is the protection factor of each barrier. The protection factor is defined as the free-field exposure rate divided by the total exposure rate inside the barrier. The total exposure rate was obtained by summing the results of the four components.

Given in Appendix A are the flux energy distributions and the exposure rate angle distributions in differential form for each component. The results are given for each of 8 energy groups and 18 ten-degree polar angle groups. The results are integrated over azimuthal angle.

In a previous study,[7] protection factors were calculated for 20-, 40-, and 80-psf cylindrical barriers using the COHORT Monte Carlo procedure.[10] The barriers had no partitions, but the barrier configuration, source, and detector were the same as used in this study. These results are used as a basis for comparison in determining the effects of the partitions and also as illustrations of limiting conditions for barriers with partitions, as described below. These results are given in Table V for 20-, 40-, and 80-psf barriers and as interpolated for a 60-psf barrier. The exposure rates are given for the direct-beam component and the barrier-scattered component. The scattered component corresponds to the sum of the scattered components in Table IV. The protection factors are given for each barrier.

Table IV. Penetration Data for Concentric Cylindrical Barriers Exposed to Infinite Plane ^{60}Co Source

(R/hr per source photon/cm^2-sec)

Radiation Component	Barrier Thickness (psf)					
	20	40	80	20	40	80
	2.5-ft Partition Radius			5.0-ft Partition Radius		
			20 - psf Partition			
EDB - IDB	1.294-6*	7.135-7	2.231-7	1.294-6	7.135-7	2.231-7
EBS - IDB	2.638-7	2.650-7	1.961-7	2.612-7	2.844-7	1.704-7
EDB - IBS	3.276-7	3.203-7	6.320-8	3.576-7	2.602-7	6.385-8
EBS - IBS	2.879-7	2.443-7	1.297-7	1.737-7	1.705-7	9.235-8
Total	2.173-6	1.543-6	6.122-7	2.087-6	1.429-6	5.497-7
Protection Factor **	2.756	3.880	9.782	2.870	4.191	10.895
			40 - psf Partition			
EDB - IDB	7.135-7	4.053-7	1.250-7	7.135-7	4.053-7	1.250-7
EBS - IDB	1.310-7	1.351-7	7.402-8	1.279-7	1.548-7	7.539-8
EDB - IBS	5.509-7	2.580-7	8.356-8	5.091-7	3.076-7	7.103-8
EBS - IBS	1.254-7	2.415-7	1.294-7	1.443-7	2.094-7	8.696-8
Total	1.521-6	1.040-6	4.119-7	1.495-6	1.077-6	3.603-7
Protection Factor	3.936	5.765	14.540	4.006	5.565	16.622

* Read 1.294-6 as 1.294×10^{-6}.

** $D_o = 5.989\text{-}6$ (R/hr per source photon/cm^2-sec).

TABLE V. Penetration Data for Simple Cylindrical Barriers Exposed to Infinite Plane ^{60}Co Source

(R/hr per source photon/cm^2-sec)

Radiation Component	Barrier Thickness (psf)			
	20	40	60*	80
Direct Beam	2.332-6**	1.294-6	7.135-7	4.053-7
Scattered	7.343-7	8.214-7	7.370-7	4.848-7
Total	3.066-6	2.116-6	1.451-6	8.901-7
Protection Factor	1.954	2.830	4.125	6.734

* The scattered component for 60 psf was obtained by interpolation of the 20-, 40-, and 80-psf data.

** Read 2.332-6 as 2.332×10^{-6}.

The 40-, 60-, and 80-psf data are used in the analysis as barriers with pseudo partitions having a radius of approximately 10 ft. This is possible by considering the 80-psf barrier, with the 10-ft outer radius, to consist of two adjacent 40-psf, concentric barriers. Therefore, the 80-psf data is the same as that for a 40-psf barrier with a 40-psf partition. Similarly, the 60-psf data are used for 20- and 40-psf barriers with 40- and 20-psf partitions, respectively.

4.1 Analysis of Components

Before considering the protection factors, it is advantageous to examine first the effects of the partitions on the various exposure rate components considered in the protection factor calculations. It is also of interest to determine the effects of the partitions on the energy and angle distributions of the flux inside the barriers.

It is suggested in Reference 6 that the Engineering Method overestimates the direct-beam component and underestimates the scattered components by approximately equal amounts. Thus, it was concluded that, although the overall results were reasonably good, the Engineering Method

appeared to be in error. Comparisons of these components of the Monte Carlo and Engineering Method data presented in Tables IV and V and Table III, respectively, indicate just the opposite. As an example, for a 40-psf barrier with no partition, the Engineering Method overpredicts the importance of the scattered components by as much as 62 percent while underpredicting the direct beam by as much as 40 percent.

In the Engineering Method, the importance of the barrier-scattered component is assumed to be independent of the partition thickness. However, the Monte Carlo data (Table IV) indicate that this component increases from 24, 39, and 55 percent of the total exposure for a 20-, 40-, and 80-psf barrier, respectively, to 53, 61, and 70 percent for barriers with 40-psf partitions.

For the 40-psf partition, the Engineering Method was found to underpredict the Monte Carlo data by as much as 18 percent for the 20-psf barrier. The largest overprediction was only 21.5 percent. Despite the improvement in the comparisons for the barriers with partitions, the large differences noted for the barriers without partitions are unexplained and should be investigated. From the results of this and previous studies,[7,8] no conclusive explanation for these differences can be made.

In the analysis of the overall results, it is important to have some indication of the importance of the various barrier-scattered components. First, consider the barriers with the 20-psf partitions. The EBS-IDB component ranges from 12 to 32 percent of the total exposure rate for the 20- to 80-psf barriers with both the 2.5- and 5.0-ft partition radius. For both partition radii, the EDB-IBS components range from 15 to 17, 18 to 21, and 10 to 12 percent for the 20-, 40-, and 80-psf barriers, respectively. For the 2.5-ft partition radius, the EBS-IBS component accounted for 13 and 21 percent of the total exposure inside the 20- and 80-psf barrier, respectively. Corresponding percentages of only 8 and 17 percent were found with a partition radius of 5.0 ft. This component shows a definite decrease in importance as the partition radius is increased.

For the 40-psf interior partition, the EDB-IBS and EBS-IBS components show a definite increase in their importance to the total exposure. This is as would be expected and, in some cases, the increase is as large as a factor of 2. However, the overall differences among the various components remains about the same as for the 20-psf partition.

For both the 20- and 40-psf partition, no individual barrier-scattered component was consistently an extremely important component. The importance of a scattered component may vary greatly from configuration to configuration.

Comparisons were made of the flux energy distributions and the exposure rate polar angle distributions of the sum of all radiation components inside the cylindrical barriers both with and without partitions. Figure 3 shows the angle distribution inside a 20-psf barrier both without a partition and with a 40-psf partition at 2.5-ft radius. The angle distribution is not as peaked around 90 degrees for the configuration with the partition as it is without the partition. The difference, which is slight, was found for both 20- and 40-psf partitions and all barrier thicknesses. No appreciable difference was found between the angle distributions inside the barriers with a 5-ft radius partition and that inside corresponding barriers without partitions.

The energy spectra inside a 40-psf barrier both with and without a partition are shown in Figure 4. The 40-psf partition has a radius of 5.0 ft. The energy spectrum is slightly harder for the configuration with the partition. This was also found true for the other configurations considered (see Appendix A).

4.2 Effect on Protection Factor of Partition Location

Given in Tables IV and V are the protection factors for 20- and 40-psf barriers with 20- and 40-psf partitions having radii of 2.5, 5.0, and 10.0 ft. These protection factors are plotted versus partition radius in Figure 5. Inspection of the protection factors indicates no consistent dependence upon the partition radius, with the exception that the protection factors are always higher for the 10-ft radius than for the 2.5-ft radius. For the

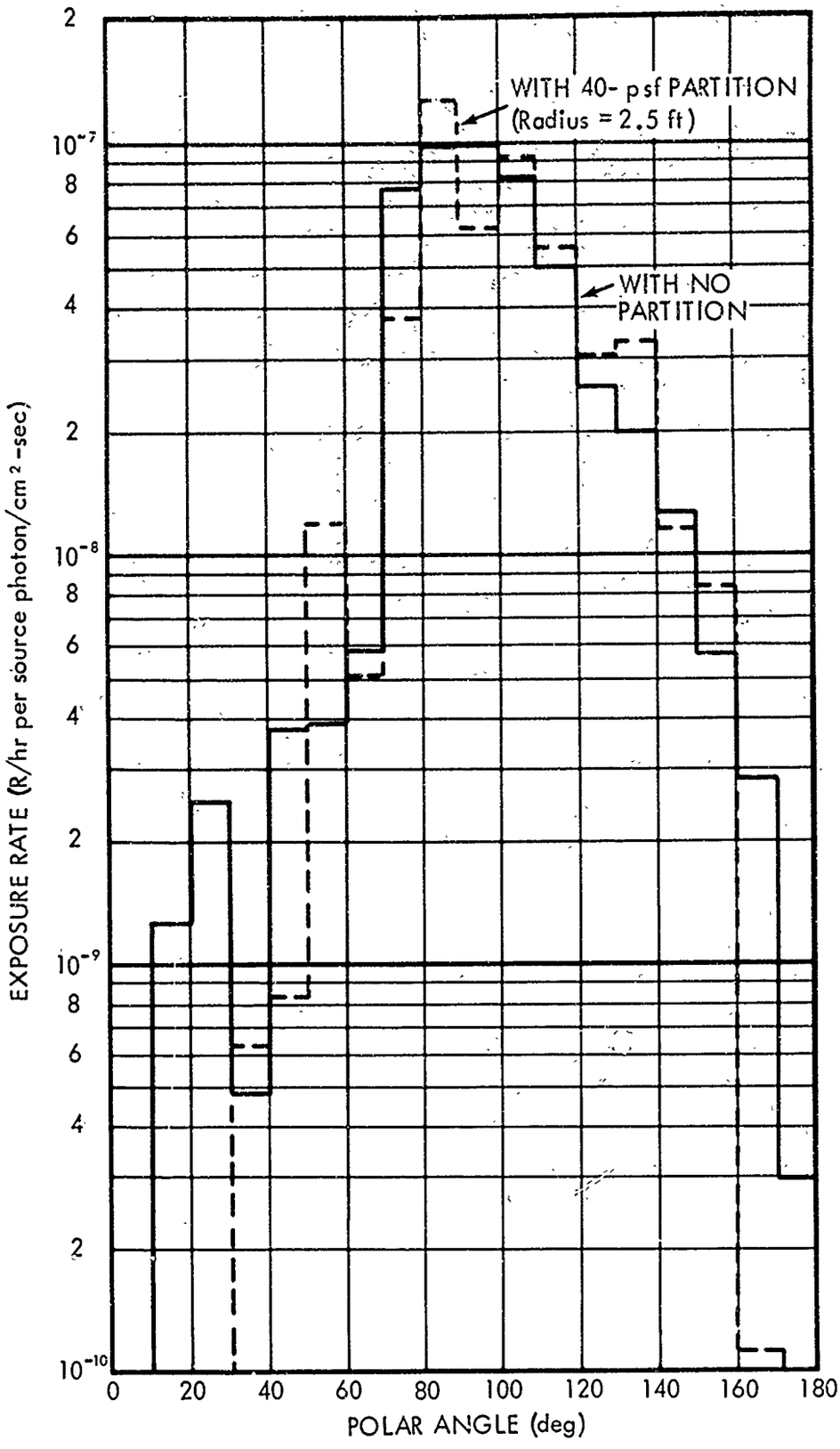

Fig. 3. Angle Distribution of the Scattered Exposure Rate Inside a 20-psf Barrier with and without 40-psf Partition

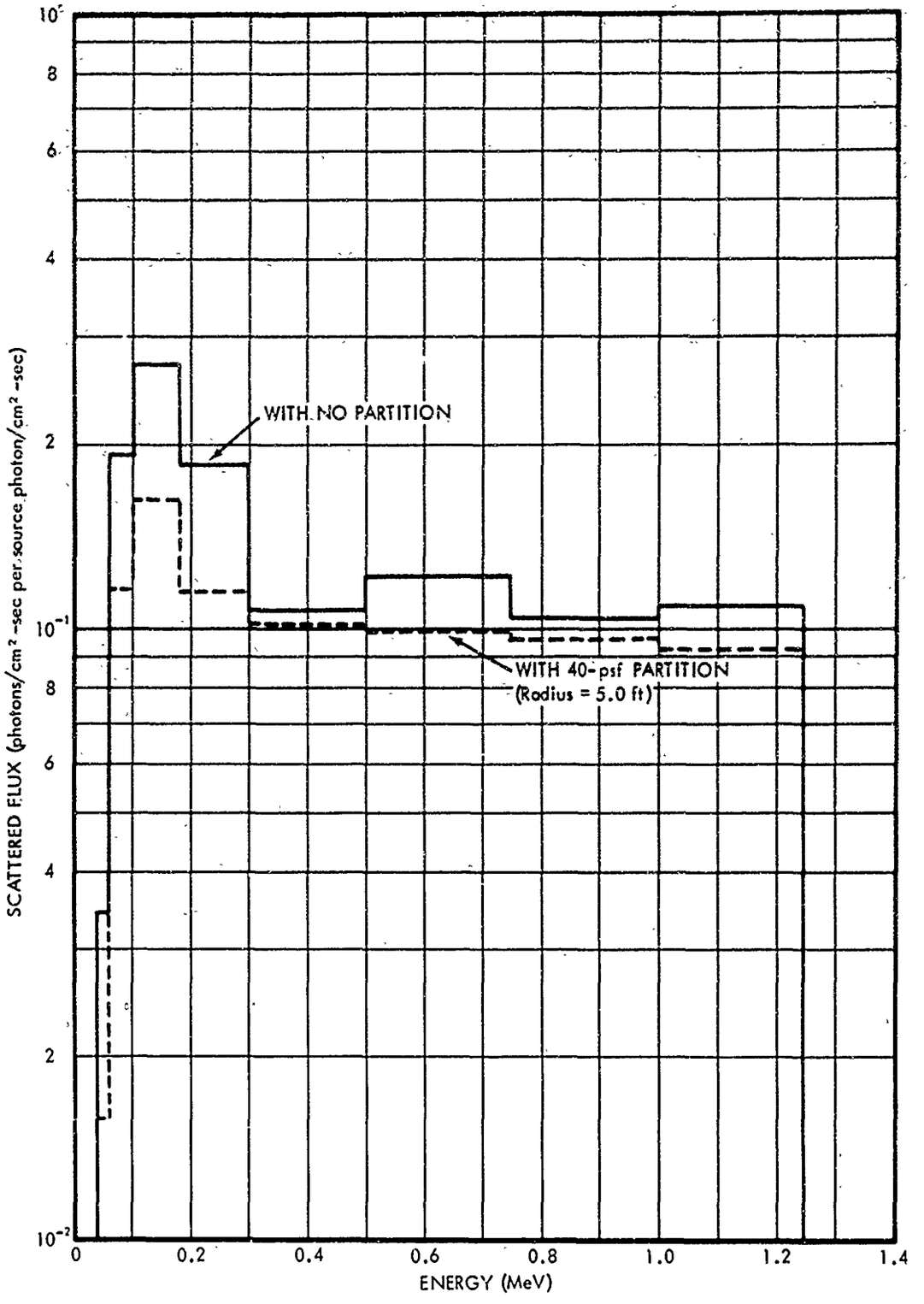

Fig. 4. Scattered Flux Energy Distribution Inside a 40-psf Barrier with and without 40-psf Partition

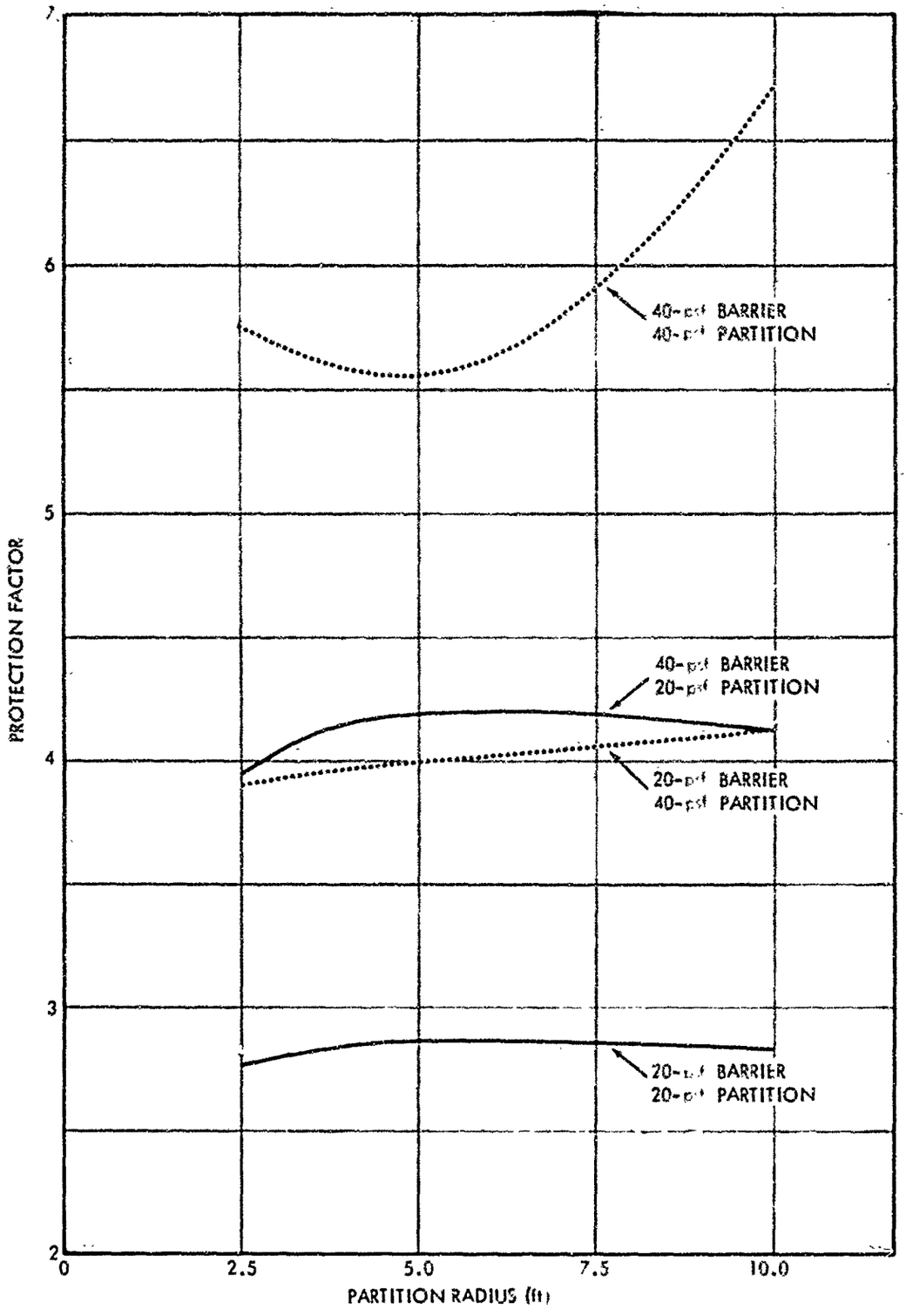

Fig. 5. Protection Factor vs. Partition Radius for Concentric Cylindrical Barriers

80-psf barrier, the protection factors were determined only for the 2.5- and 5.0-ft partition radius. These data indicate that the protection factors for the 5.0-ft radius are higher than those for the 2.5-ft radius by 11 and 14 percent for the 20- and 40-psf partitions, respectively. The Engineering Method is independent of the partition location.

Examination of the barrier-scattered components indicated that only the EBS-IBS component shows any consistent dependence upon the partition location. This component varies from 8 to 31 percent of the total exposure rate. With one exception, the exposure rates due to the EBS-IBS component for the 2.5-ft partition radius are 30 to 40 percent higher than for the 5.0-ft configuration. For the 20-psf barrier with the 40-psf partition, the exposure rate is 13 percent less for the 2.5-ft data. The 2.5-ft data appears to be somewhat low. The data for the 10.0-ft configuration were calculated for the total barrier-scattered component only.

It is concluded that for barrier thicknesses and configurations where the EBS-IBS component is the principle component, the protection factor is reduced as the partition is placed closer to the detector position. However, for barrier and partition thicknesses and radii within the range used in this study, the location of the partition can be neglected. This conclusion is in agreement with the assumptions used in the Engineering Method. Any error introduced into the results by neglecting the partition location is on the conservative side.

4.3 Effect on Protection Factor of Barrier and Partition Thickness

The Monte Carlo protection factors are plotted versus exterior barrier thickness in Figure 6. Also shown are experimental results which will be discussed in Section 4.4.

With no partition, the protection factor for an 80-psf barrier is a factor of 3.45 larger than that for a 20-psf barrier. With 40-psf partitions, the protection factor for the 80-psf barrier is as much as a factor of 4.15 greater than for the 20-psf barrier. This increase of approximately 20 percent appears to be due mainly to the changes in the EDB-IBS component. As

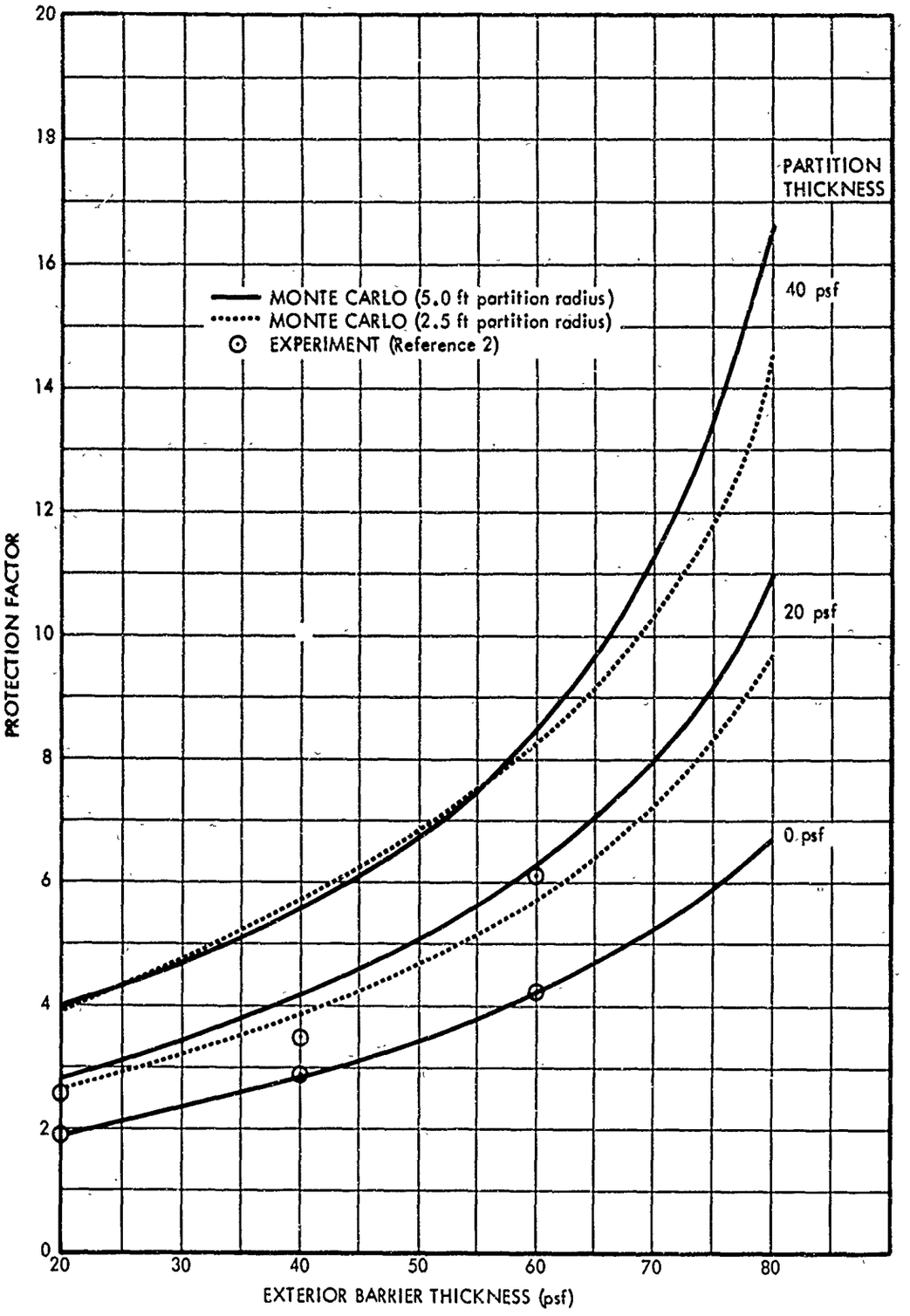

Fig. 6. Protection Factor vs. Exterior Barrier Thickness for Concentric Cylindrical Barriers

indicated in Table IV, this component increases approximately 27.5 percent more for a 20-psf barrier than for an 80-psf barrier when the partition thickness is increased from 20 to 40 psf. The same effect was found for partition radii of 2.5 and 5.0 ft.

With 40-psf partitions, the protection factors for the various barrier thicknesses and partition radii ranged from a factor of 1.97 to 4.27 larger than the protection factors for corresponding barriers with no partitions. Overall, these factors show a slight increase for the 40-psf partition thickness as the exterior barrier thickness is increased. However, as the barrier thickness was increased from 20- to 80-psf, there was less than a 26 percent difference between the largest and smallest increase in the protection factors due to the addition of the partition. This small variation suggests that perhaps some average barrier reduction factor could be used for the partitions. It would be a function only of the partition thickness, a fact which is consistent with the neglect of the exterior barrier thickness in the Engineering Method.

4.4 Comparisons of Monte Carlo, Experimental, and Engineering Method Protection Factors

It is assumed in the Engineering Method that the protection factor for a barrier with a partition is independent of location of the partition. It is also assumed that the barrier reduction factor for the partition is a function only of the partition thickness. Using Monte Carlo data in the preceding sections, these assumptions were found to be sound. However, verification of the assumptions gives no indication of the overall ability of the Engineering Method to predict the protection factor of a barrier with a partition. Comparisons between the Monte Carlo and Engineering Method protection factors will be used to determine the ability of the Engineering Method to predict protection factors. The Monte Carlo protection factors are compared with similar measured data before using them as a basis of comparison.

Technical Operations, Inc., conducted an experiment in which scale models were exposed to a ^{60}Co source.[2] One of the scale models was a cylindrical steel barrier 2 ft in height and 1 ft in radius with an interior

partition 0.5 ft in radius. The ^{60}Co source simulated a uniformly contaminated infinite plane of gamma radiation and was comparable to the source term assumed in the present penetration calculations. Because the barriers were not of infinite height, the exposure rates inside the barriers contained a skyshine component which is not present in the Monte Carlo results. To allow a direct comparison, the skyshine, through the open top, was removed by subtracting an Engineering Method estimate of this component.

The adjusted measured results for a detector height of 3 in. were used to calculate protection factors for model barriers of various thicknesses. The 3-in. data were used because the solid angle fractions subtended at this height were closest to those for which the calculations were made. The resulting protection factors are compared with the Monte Carlo protection factors in Figure 6.

The results agree within 3.5 percent for the barriers with no interior partitions. For the barriers with a 20-psf partition, the Monte Carlo results for the 5.0-ft-radius partition agree with the measured results within 20 percent and the Monte Carlo results for the 2.5-ft-radius partition agree within 10 percent. The 5.0-ft-radius partition was expected to give the best comparison since the two geometries are more comparable. The total attenuation afforded by the partitions was found to be generally 15 to 20 percent less for the measured data than for the Monte Carlo data. Differences of this magnitude could be due to the different barrier configurations and sources used.

Figures 7, 8, and 9 show comparisons of the protection factors at a height of 3 ft inside the 20-, 40-, and 80-psf barriers, respectively, with 0-, 20-, and 40-psf partitions calculated by Monte Carlo and by the Engineering Method. Included in the comparisons are the results of the Engineering Method calculations using a barrier reduction factor based on the Monte Carlo data. These special calculations will be described below.

The agreement between the Monte Carlo and the regular Engineering Method calculations is reasonably good in both shape and magnitude with the largest difference being approximately 22 percent for the 40-psf barrier

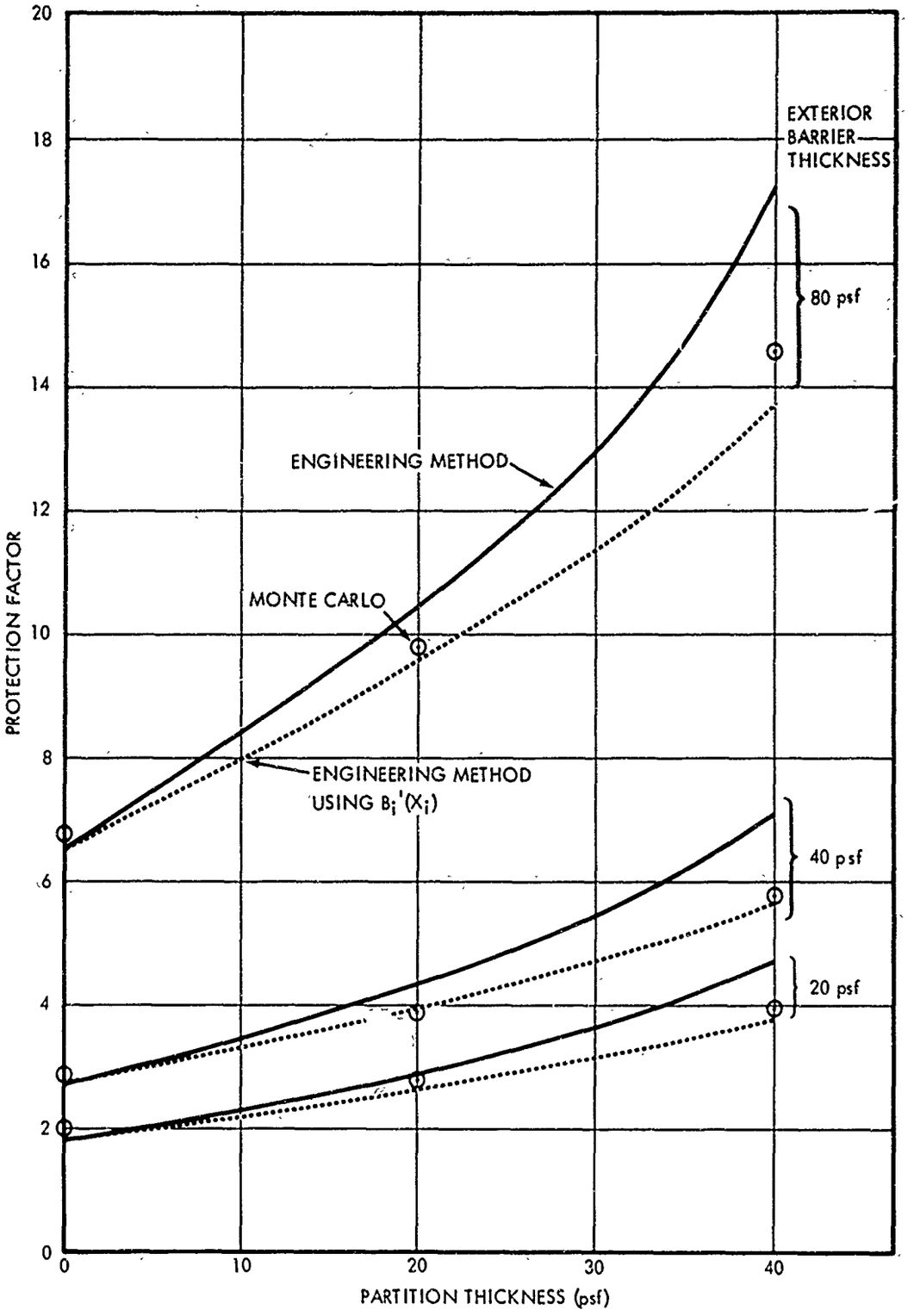

Fig. 7. Protection Factor vs. Partition Thickness for Concentric Cylindrical Barriers (Partition Radius = 2.5 ft)

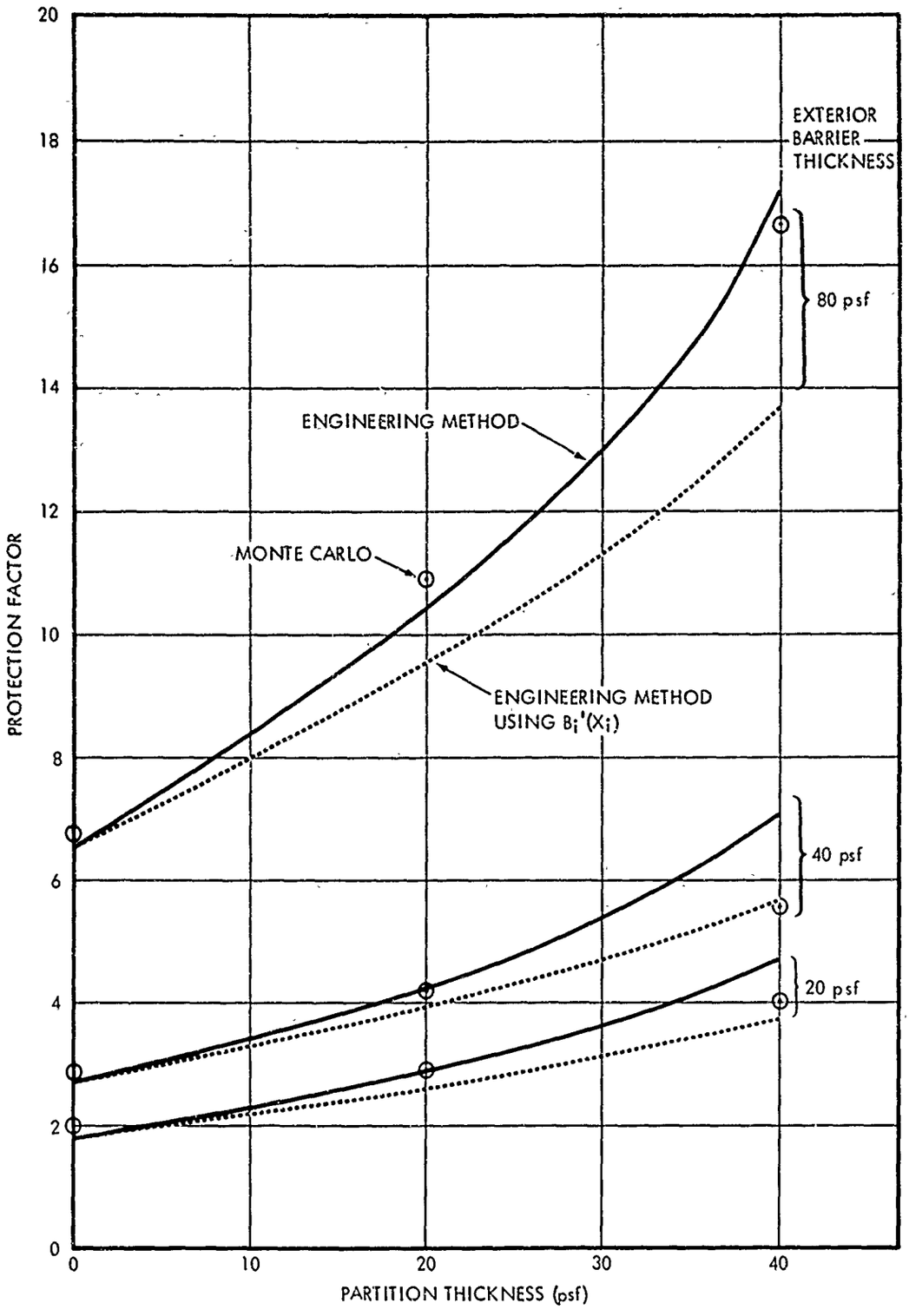

Fig. 8. Protection Factor vs. Partition Thickness for Concentric Cylindrical Barriers (Partition Radius = 5.0 ft)

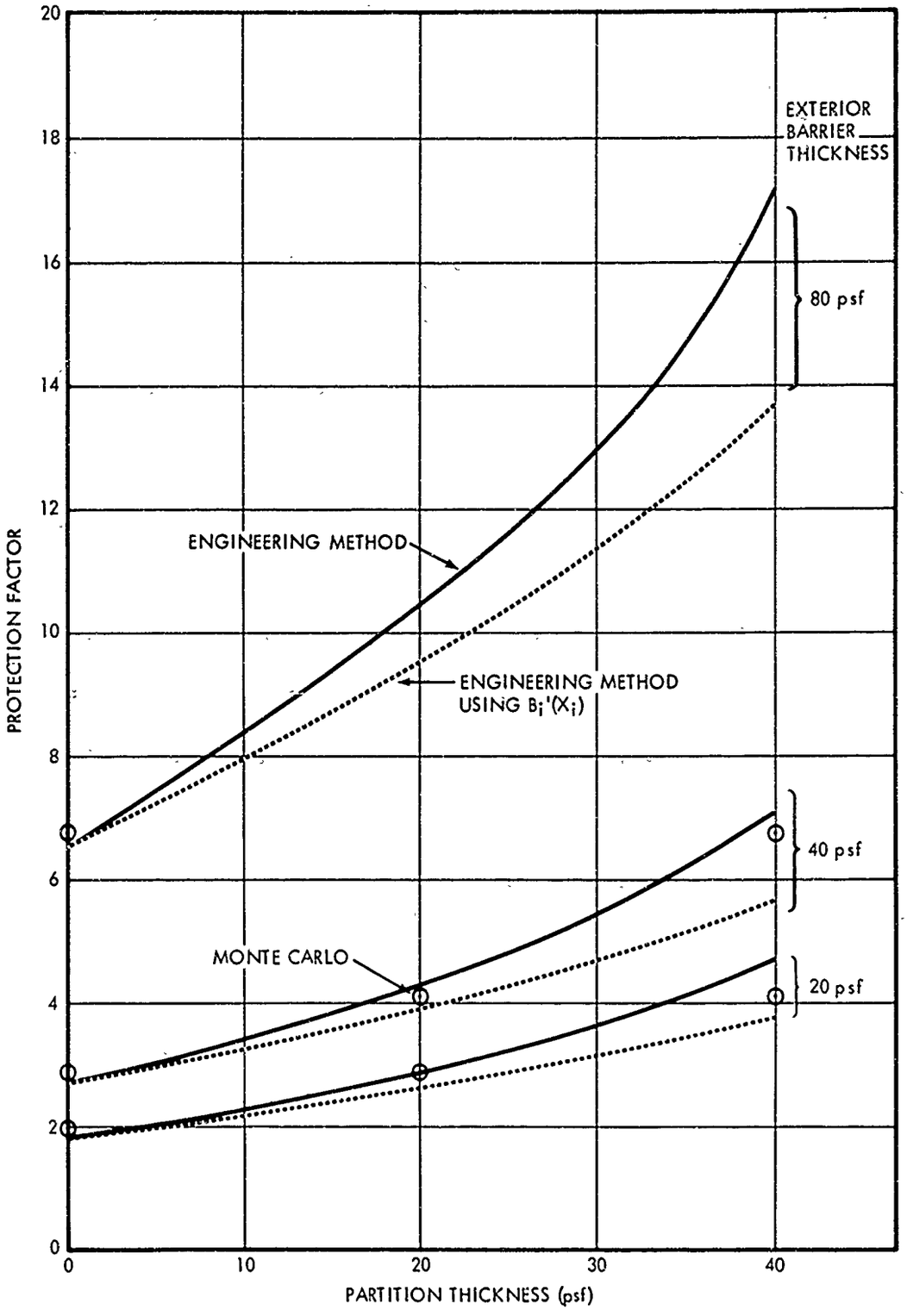

Fig. 9. Protection Factor vs. Partition Thickness for Concentric Cylindrical Barriers (Partition Radius = 10.0 ft)

with a 40-psf partition at a radius of 5.0 ft. The results for the 20-psf barrier with a 20-psf partition agree within 1 percent. The average difference for all barrier configurations is 7.7 percent. Overall, the agreement is generally better for the barriers with the thinner interior partitions. However, as pointed out in Section 4.1, the best agreement between the Monte Carlo and the Engineering Method results for the barrier-scattered component was found for the thicker interior partitions.

The increased disagreement observed as the interior barrier becomes more important indicates: 1) that the barrier factors assumed for the interior partitions are incorrect, or 2) that the method to account for the partition is incorrect. As indicated by all previous experimental studies [1,2,3] as well as in Figures 7, 8, and 9, the protection factors predicted by the Engineering Method are nonconservative. Thus, it seems desirable to modify the Engineering Method to give improved agreement or, at least, a conservative prediction.

Since the preceding analysis suggests that the assumptions used in the Engineering Method are not unreasonable, it was decided to try to improve the interior partition barrier factors. The Monte Carlo reduction factors for a given barrier with a partition was divided by that for the same barrier with no partition to obtain Monte Carlo barrier reduction factors. As a result, six new barrier reduction factors were determined for each partition thickness (i.e., one for each of the three external barrier thicknesses and for both the 2.5 and 5.0-ft radius partition).

As suggested in Section 4.3, an average barrier reduction factor was determined for each partition thickness by averaging the six new barrier reduction factors. The average Monte Carlo barrier reduction factor, $B_i'(X_i)$, was found to be larger than the original factors, $B_i(X_i)$, (see Section III) by 0, 9, and 25 percent for 0-, 20-, and 40-psf partitions, respectively. It should be noted, however, that the shape of the partition is accounted for in the $B_i'(X_i)$ terms. The shape of the partition is not considered in the Engineering Method.

Figures 7, 8, and 9 include a comparison with Engineering Method results obtained by replacing $B_i(X_i)$ with $B_i'(X_i)$. The agreement is somewhat

improved between the Monte Carlo and the new Engineering Method results, and, in addition, the new Engineering Method results are generally conservative.

Recall that the Engineering Method accounts for the partition by adjusting the reduction factor for a barrier with no partition by a barrier reduction factor which is a function only of partition thickness. The same reduction factor curves are used for both the barrier and the partition. The results and improvements observed above indicate that the Engineering Method may be adequate if separate data are used for the interior partition reduction factors.

Changing the Engineering Method to incorporate separate barrier reduction factor data for the partitions would involve only the addition of $B_i'(X_i)$ data to an existing barrier reduction factor chart (i.e., Chart 1, Reference 4).

V. CONCLUSIONS

The main objectives of this study were to determine the effects of partitions in fallout shielding and the ability of the Engineering Method to predict such effects. Monte Carlo procedures were used to calculate the exposure rate inside 20-, 40-, and 80-psf cylindrical barriers with 0-, 20-, and 40-psf interior partitions. The radius of the cylindrical barriers was 10.0 ft. The barriers were exposed to an infinite plane ^{60}Co source. Engineering Method calculations were also made to determine the effects of the interior partitions.

The final results of the calculations were expressed in the form of a protection factor for each barrier. An analysis of the Monte Carlo data was made to determine the effects of the partition. The Monte Carlo and Engineering Method protection factors were compared to determine the ability of the Engineering Method to predict such effects.

The Monte Carlo protection factors showed no consistent dependence upon the location of the partition. Overall, the protection factor increased an average of 8.0 percent as the radius increased from 2.5 to 10.0 ft. The location becomes more important as the barrier or partition thickness is increased. Over the range of radii and barrier thicknesses used here, it was concluded that the location of the partition is unimportant. The neglect of the location of the partition in the Engineering Method is consistent with this conclusion.

The 40-psf partition increased the protection factors of the various barrier configurations by factors ranging from 1.97 to 2.47. The increases were all the same within 26 percent. This indicates that some average barrier reduction factor which is a function only of the partition thickness could be used in calculating the effect of the partition. This is consistent with the Engineering Method in that the partition barrier reduction factor is assumed to be a function only of the partition thickness.

The Monte Carlo and Engineering Method protection factors were compared. The average difference was 7.7 percent, with the largest difference approximately 22 percent. The Engineering Method results were generally higher. This same trend was also noted in previous experimental studies.

Average barrier reduction factors for the interior partitions were calculated from the Monte Carlo data for each partition thickness. The results were found to be larger than similar Engineering Method data by 0, 9, and 25 percent for 0-, 20-, and 40-psf partitions.

The new barrier reduction factors were used in additional Engineering Method calculations. The results were compared with Monte Carlo protection factors and found to agree much better than did the original Engineerng Method data. Also, the new results were on the conservative side of the Monte Carlo protection factors.

It was concluded that the assumptions used in the Engineering Method for predicting the effects of interior partitions in fallout shielding are reasonable. However, new barrier reduction factors should be calculated for the partitions. At present, the same barrier reduction factor curves are used for both the exterior barriers and the partitions.

Before incorporating new partition barrier reduction factors, it would be necessary to extend the range of the barrier and partition thicknesses and locations considered in this study to determine the exact range for which the assumptions used in the Engineering Method are valid. It would also be necessary to determine the exact dependence of $B_i'(X_i)$ on the geometric shape of the partition. It should be noted that these conclusions are based only on cylindrical geometries and may not apply to other geometries.

REFERENCES

1. A. W. Starbird et al., The Effect of Interior Partitions on the Dose Rate in a Multistory, Windowless Building, TO-B 63-6 (January 1963).

2. A. L. Kaplan et al., Final Report - Phase I: Structure Shielding from Simulated Fallout Gamma Radiation, TO-B 65-27 (November 1965).

3. J. D. Velletri et al., Protection Factors of Emergency Shelters in a British Residence, TO-B 63-41 (November 1963).

4. Design and Review of Structures for Protection from Fallout Gamma Radiation, OCD PM-100-1, Interim Edition (1965).

5. L. V. Spencer, Structure Shielding Against Fallout Radiation from Nuclear Weapons, NBS Monograph 42 (June 1962).

6. J. F. Batter and A. W. Starbird, The Preparation of Simplified Manuals for Shielding Analysis, CONESCO Report No. 4848-1 (March 1967).

7. R. L. French et al., Monte Carlo Study of Structure Shielding Against Fallout Radiation, RRA-T73 (March 1967).

8. R. L. French et al., Ground Roughness Effects on Fallout Shielding, RRA-T81 (January 1968).

9. J. H. Price, GRASS, A Monte Carlo Procedure for Calculating Gamma-Ray Attenuation of Simple Structures, RRA-T79 (December 1967).

10. D. G. Collins and M. B. Wells, COHORT, A Monte Carlo Program for Calculation of Radiation Heating and Transport, Vols. I-IV, RRA-T62 (September 1966).

11. Theodore Rockwell III, Editor, Reactor Shielding Design Manual, D. Van Nostrand Company.

12. Gladys White Grodstein, X-ray Attenuation Coefficients from 10 KeV to 100 MeV, National Bureau of Standards Circular 583 (1957) with Supplement (1959).

13. C. Eisenhauer, An Engineering Method for Calculating Protection Afforded by Structures Against Fallout Radiation, NBS Monograph 76 (July 1964).

APPENDIX A

Gamma-Ray Energy and Angle Distributions Inside Concentric Cylindrical Barriers Exposed to Infinite Plane ^{60}Co Source

Table		Page
A1	Flux Energy Distribution Inside 20-, 40-, and 80-psf Barriers with a 20-psf Partition at a 2.5-ft Radius	38
A2	Flux Energy Distribution Inside 20-, 40-, and 80-psf Barriers with a 20-psf Partition at a 5.0-ft Radius	39
A3	Flux Energy Distribution Inside 20-, 40-, and 80-psf Barriers with a 40-psf Partition at a 2.5-ft Radius	40
A4	Flux Energy Distribution Inside 20-, 40-, and 80-psf Barriers with a 40-psf Partition at a 5.0-ft Radius	41
A5	Exposure Rate Angle Distribution Inside a 20-psf Barrier with a 20-psf Partition	42
A6	Exposure Rate Angle Distribution Inside a 40-psf Barrier with a 20-psf Partition	43
A7	Exposure Rate Angle Distribution Inside a 80-psf Barrier with a 20-psf Partition	44
A8	Exposure Rate Angle Distribution Inside a 20-psf Barrier with a 40-psf Partition	45
A9	Exposure Rate Angle Distribution Inside a 40-psf Barrier with a 40-psf Partition	46
A10	Exposure Rate Angle Distribution Inside a 80-psf Barrier with a 40-psf Partition	47

NOTE: The distributions are listed in terms of the upper bounds of the energy and angle groups; the lower bound is 0.04 MeV for the first energy group and 0° for the first angle group.

TABLE A1. Flux Energy Distribution Inside 20-, 40-, and 80-psf Barriers with a 20-psf Partition at a 2.5-ft Radius

(photons/cm^2-sec per source photon/cm^2-sec)

Energy	Radiation Component				
(Mev)	EDB-IBS	EBS-IDB	EBS-IBS	EDB-IDB	Total
		20-psf Barrier Thickness			
0.06	4.857-03*	2.346-04	2.946-02	0.000-00	3.455-02
0.10	2.589-02	6.888-03	1.429-01	0.000-00	1.757-01
0.18	9.412-02	2.657-02	2.089-01	0.000-00	3.296-01
0.30	9.505-02	3.228-02	1.034-01	0.000-00	2.307-01
0.50	3.893-02	3.092-02	1.070-01	0.000-00	1.769-01
0.75	6.724-02	4.110-02	4.947-02	0.000-00	1.578-01
1.00	1.936-02	4.651-02	1.099-02	0.000-00	7.686-02
1.25	5.144-02	4.035-02	0.000-00	5.953-01	6.871-01
Total	3.969-01	2.248-01	6.525-01	5.953-01	1.869-00
		40-psf Barrier Thickness			
0.06	4.296-03	3.232-04	1.306-02	0.000-00	1.768-02
0.10	5.636-02	7.191-03	1.065-01	0.000-00	1.701-01
0.18	9.762-02	2.590-02	1.487-01	0.000-00	2.722-01
0.30	1.018-01	2.957-02	9.015-02	0.000-00	2.215-01
0.50	4.513-02	3.235-02	6.569-02	0.000-00	1.432-01
0.75	2.992-02	4.795-02	2.460-02	0.000-00	1.025-01
1.00	3.131-02	4.225-02	3.960-02	0.000-00	1.132-01
1.25	5.494-02	4.027-02	0.000-00	3.233-01	4.185-01
Total	4.215-01	2.258-01	4.885-01	3.233-01	1.459-00
		80-psf Barrier Thickness			
0.06	7.089-04	1.624-04	6.121-03	0.000-00	6.992-03
0.10	8.620-03	3.370-03	8.517-02	0.000-00	9.716-02
0.18	1.142-02	1.558-02	1.098-01	0.000-00	1.368-01
0.30	1.629-02	1.334-02	5.027-02	0.000-00	7.990-02
0.50	9.387-03	1.515-02	2.369-02	0.000-00	4.823-02
0.75	1.343-02	3.000-02	3.551-02	0.000-00	7.894-02
1.00	1.575-02	2.681-02	2.219-03	0.000-00	4.478-02
1.25	0.000-00	4.264-02	1.957-04	9.911-02	1.419-01
Total	7.563-02	1.470-01	3.131-01	9.911-02	6.347-01

* Read 4.857-03 as 4.857×10^{-3}.

TABLE A2. Flux Energy Distribution Inside 20-, 40-, and 80-psf Barriers with a 20-psf Partition at a 5.0-ft Radius

(photons/cm^2-sec per source photon/cm^2-sec)

Energy	Radiation Component				
(Mev)	EDB-IBS	EBS-IDB	EBS-IBS	EDB-IDB	Total
		20-psf Barrier Thickness			
0.06	1.792-02	1.918-04	2.469-02	0.000-00	4.282-02
0.10	9.246-02	6.781-03	1.044-01	0.000-00	2.036-01
0.18	1.273-01	2.784-02	1.466-01	0.000-00	3.019-01
0.30	8.717-02	2.831-02	6.976-02	0.000-00	1.852-01
0.50	6.682-02	3.136-02	6.047-02	0.000-00	1.586-01
0.75	5.617-02	4.419-02	2.760-02	0.000-00	1.279-01
1.00	4.436-02	3.875-02	3.592-03	0.000-00	8.671-02
1.25	3.407-02	4.414-02	0.000-00	5.953-01	6.735-01
Total	5.263-01	2.215-01	4.373-01	5.953-01	1.780-00
		40-psf Barrier Thickness			
0.06	3.919-03	2.408-04	2.005-02	0.000-00	2.421-02
0.10	3.804-02	8.313-03	1.145-01	0.000-00	1.609-01
0.18	4.817-02	2.577-02	1.659-01	0.000-00	2.398-01
0.30	4.081-02	3.012-02	7.164-02	0.000-00	1.426-01
0.50	2.827-02	3.619-02	5.551-02	0.000-00	1.200-01
0.75	4.026-02	5.088-02	1.965-02	0.000-00	1.108-01
1.00	2.676-02	4.121-02	6.503-03	0.000-00	7.447-02
1.25	4.994-02	4.697-02	0.000-00	3.233-01	4.202-01
Total	2.762-01	2.396-01	4.539-01	3.233-01	1.293-00
		80-psf Barrier Thickness			
0.06	9.319-04	1.472-04	3.746-03	0.000-00	4.825-03
0.10	6.712-03	3.950-03	3.613-02	0.000-00	4.679-02
0.18	1.355-02	1.361-02	5.747-02	0.000-00	8.463-02
0.30	1.521-02	1.205-02	4.600-02	0.000-00	7.326-02
0.50	6.828-03	1.628-02	2.087-02	0.000-00	4.398-02
0.75	1.043-02	3.376-02	2.796-02	0.000-00	7.215-02
1.00	4.507-03	2.918-02	9.910-07	0.000-00	3.369-02
1.25	1.249-02	2.606-02	0.000-00	9.911-02	1.376-01
Total	7.068-02	1.350-01	1.921-01	9.911-02	4.969-01

TABLE A3. Flux Energy Distribution Inside 20-, 40-, and 80-psf Barriers with a 40-psf Partition at a 2.5- ft Radius

(photons/cm^2-sec per source photon/cm^2-sec)

Energy	Radiation Component				
(Mev)	EDB-IBS	EBS-IDB	EBS-IBS	EDB-IDB	Total
		20-psf Barrier Thickness			
0.06	5.801-03	7.660-06	8.566-03	0.000-00	1.437-02
0.10	8.806-02	8.600-04	6.256-02	0.000-00	1.515-01
0.18	1.489-01	4.948-03	9.367-02	0.000-00	2.475-01
0.30	8.434-02	6.939-03	5.666-02	0.000-00	1.479-01
0.50	7.389-02	9.415-03	4.009-02	0.000-00	1.234-01
0.75	1.305-01	1.728-02	2.742-02	0.000-00	1.752-01
1.00	7.656-02	2.164-02	4.032-04	0.000-00	9.860-02
1.25	5.077-02	2.852-02	0.000-00	3.233-01	4.026-01
Total	6.589-01	8.961-02	2.893-01	3.233-01	1.361-00
		40-psf Barrier Thickness			
0.06	3.546-03	9.400-06	7.144-03	0.000-00	1.070-02
0.10	3.576-02	7.923-04	5.096-02	0.000-00	8.751-02
0.18	4.794-02	4.711-03	1.332-01	0.000-00	1.859-01
0.30	4.383-02	8.992-03	8.066-02	0.000-00	1.335-01
0.50	3.587-02	1.169-02	5.981-02	0.000-00	1.074-01
0.75	4.179-02	1.990-02	5.159-02	0.000-00	1.133-01
1.00	4.202-02	2.524-02	2.968-02	0.000-00	9.694-02
1.25	3.198-02	2.459-02	2.690-04	1.783-01	2.351-01
Total	2.827-01	9.594-02	4.134-01	1.783-01	9.703-01
		80-psf Barrier Thickness			
0.06	1.399-03	4.485-06	2.308-03	0.000-00	3.711-03
0.10	9.232-03	5.465-04	4.464-02	0.000-00	5.442-02
0.18	1.322-02	3.316-03	7.315-02	0.000-00	8.969-02
0.30	2.116-02	4.379-03	5.392-02	0.000-00	7.946-02
0.50	6.579-03	5.693-03	1.573-02	0.000-00	2.800-02
0.75	1.460-02	8.892-03	5.481-03	0.000-00	2.897-02
1.00	4.783-03	1.399-02	3.609-02	0.000-00	5.486-02
1.25	1.779-02	1.488-02	0.000-00	5.530-02	8.797-02
Total	8.877-02	5.171-02	2.312-01	5.530-02	4.270-01

TABLE A4. Flux Energy Distribution Inside 20-, 40-, and 80-psf Barriers with a 40-psf Partition at a 5.0-ft Radius

(photons/cm^2-sec per source photon/cm^2-sec)

Energy	Radiation Component				
(Mev)	EDB-IBS	EBS-IDB	EBS-IBS	EDB-IDB	Total
			20-psf Barrier Thickness		
0.06	7.758-03	6.521-06	7.360-03	0.000-00	1.512-02
0.10	6.046-02	7.236-04	6.672-02	0.000-00	1.279-01
0.18	1.273-01	4.402-03	9.939-02	0.000-00	2.311-01
0.30	1.083-01	7.044-03	4.885-02	0.000-00	1.642-01
0.50	6.842-02	1.053-02	3.377-02	0.000-00	1.127-01
0.75	8.142-02	1.907-02	2.250-02	0.000-00	1.230-01
1.00	6.932-02	2.091-02	8.606-03	0.000-00	9.884-02
1.25	6.803-02	2.617-02	8.642-03	3.233-01	4.261-01
Total	5.912-01	8.889-02	2.958-01	3.233-01	1.299-00
			40-psf Barrier Thickness		
0.06	6.824-03	7.637-06	8.875-03	0.000-00	1.571-02
0.10	3.801-02	8.768-04	7.677-02	0.000-00	1.157-01
0.18	5.116-02	5.120-03	1.058-01	0.000-00	1.621-01
0.30	4.283-02	7.437-03	6.366-02	0.000-00	1.139-01
0.50	4.167-02	1.091-02	4.810-02	0.000-00	1.007-01
0.75	3.858-02	1.957-02	4.044-02	0.000-00	9.859-02
1.00	5.131-02	2.024-02	2.441-02	0.000-00	9.596-02
1.25	4.732-02	3.896-02	5.530-03	1.783-01	2.701-01
Total	3.176-01	1.031-01	3.736-01	1.783-01	9.727-01
			80-psf Barrier Thickness		
0.06	1.800-03	3.327-06	6.197-03	0.000-00	8.000-03
0.10	9.793-03	4.620-04	3.181-02	0.000-00	4.207-02
0.18	1.616-02	2.560-03	4.394-02	0.000-00	6.266-02
0.30	1.600-02	3.921-03	2.458-02	0.000-00	4.450-02
0.50	6.833-03	7.405-03	1.626-02	0.000-00	3.050-02
0.75	1.382-02	1.214-02	8.697-03	0.000-00	3.466-02
1.00	1.382-02	1.162-02	2.221-02	0.000-00	4.765-02
1.25	5.465-03	1.500-02	0.000-00	5.530-02	7.577-02
Total	8.372-02	5.313-02	1.536-01	5.530-02	3.458-01

TABLE A5. Exposure Rate Angle Distribution Inside a 20-psf Barrier with a 20-psf Partition

(R/hr per source photon/cm^2-sec)

Polar Angle (deg)	Radiation Component					Radiation Component				
	EDB-IBS	EBS-IDB	EBS-IBS	EDB-IDB	Total	EDB-IBS	EBS-IDB	EBS-IBS	EDB-IDB	Total
	2.5-ft Partition Radius					5.0-ft Partition Radius				
10	0.000-00	0.000-00	1.553-10	0.000-00	1.553-10	0.000-00	0.000-00	1.016-10	0.000-00	1.016-10
20	0.000-00	0.000-00	3.888-10	0.000-00	3.888-10	1.529-09	0.000-00	1.181-09	0.000-00	2.710-09
30	2.092-09	0.000-00	2.320-09	0.000-00	4.411-09	5.440-09	0.000-00	3.179-09	0.000-00	8.619-09
40	1.890-09	0.000-00	1.149-08	0.000-00	1.339-08	1.549-09	0.000-00	3.094-09	0.000-00	4.644-09
50	5.467-11	0.000-00	3.746-09	0.000-00	3.801-09	4.910-09	0.000-00	1.926-09	0.000-00	6.836-09
60	3.734-09	0.000-00	3.430-09	0.000-00	7.163-09	2.325-09	0.000-00	4.608-09	0.000-00	6.933-09
70	2.411-08	0.000-00	1.600-08	0.000-00	4.011-08	2.989-08	0.000-00	1.107-08	0.000-00	4.097-08
80	1.785-10	3.746-08	3.777-09	1.794-07	2.208-07	8.891-08	3.326-08	8.263-09	1.794-07	3.098-07
90	4.241-08	4.630-08	3.412-08	1.057-06	1.180-06	2.716-08	6.381-08	1.575-08	1.057-06	1.164-06
100	8.450-08	5.661-08	2.745-08	3.790-08	2.065-07	1.499-08	5.766-08	2.899-08	3.790-08	1.395-07
110	8.547-08	4.844-08	2.419-08	8.610-09	1.667-07	5.772-08	4.515-08	1.890-08	8.610-09	1.304-07
120	2.995-10	3.788-08	2.037-08	4.010-09	6.256-08	3.265-08	3.027-08	1.241-08	4.010-09	7.934-08
130	2.283-08	1.971-08	2.971-08	4.310-09	7.656-08	2.719-08	1.286-08	2.492-08	4.310-09	6.928-08
140	2.082-08	1.111-08	7.016-08	1.800-09	1.039-07	2.683-08	1.103-08	1.437-08	1.800-09	5.403-08
150	1.482-08	5.214-09	1.840-08	3.700-10	3.880-08	1.489-08	6.280-09	9.067-09	3.700-10	3.061-08
160	1.490-08	1.067-09	1.407-08	1.620-11	3.005-08	1.490-08	9.189-10	1.259-08	1.620-11	2.843-08
170	7.015-09	2.682-12	6.930-09	7.620-14	1.395-08	5.927-09	3.528-12	3.223-09	7.620-14	9.154-09
180	2.439-09	0.000-00	1.182-09	0.000-00	3.621-09	2.879-10	0.000-00	7.273-11	0.000-00	3.606-10
Total	3.276-07	2.638-07	2.879-07	1.294-06	2.173-06	3.576-07	2.612-07	1.737-07	1.294-06	2.086-06

TABLE A6. Exposure Rate Angle Distribution Inside a 40-psf Barrier with a 20-psf Partition

(R/hr per source photon/cm^2-sec)

Polar Angle (deg)	Radiation Component					Radiation Component				
	EDB-IBS	EBS-IDB	EBS-IBS	EDB-IDB	Total	EDB-IBS	EBS-IDB	EBS-IBS	EDB-IDB	Total
	2.5-ft Partition Radius					5.0-ft Partition Radius				
10	3.416-10	0.000-00	6.080-11	0.000-00	4.024-10	1.519-09	0.000.00	1.352-09	0.000-00	2.871-09
20	1.268-09	0.000-00	2.321-10	0.000-00	1.500-09	7.486-10	0.000-00	4.314-10	0.000-00	1.180-09
30	3.347-09	0.000-00	7.058-10	0.000-00	4.053-09	1.788-10	0.000-00	4.884-10	0.000-00	6.673-10
40	0.000-00	0.000-00	1.811-09	0.000-00	1.811-09	7.556-10	0.000-00	3.200-09	0.000-00	3.956-09
50	2.002-08	0.000-00	1.161-08	0.000-00	3.163-08	6.283-10	0.000-00	5.015-09	0.000-00	5.643-09
60	6.634-09	0.000-00	5.905-09	0.000-00	1.254-08	8.487-10	0.000-00	3.752-09	0.000-00	4.601-09
70	2.452-08	0.000-00	4.626-08	0.000-00	7.079-08	4.065-08	0.000-00	9.376-09	0.000-00	5.003-08
80	2.771-08	2.974-08	9.572-09	9.820-08	1.652-07	4.217-08	3.914-08	1.545-08	9.820-08	1.950-07
90	1.281-07	6.929-08	8.216-09	5.895-07	7.951-07	5.282-08	6.323-08	2.406-08	5.895-07	7.296-07
100	3.313-09	4.721-08	7.681-09	1.860-08	7.680-08	3.352-08	6.558-08	1.270-08	1.860-08	1.304-07
110	1.301-08	5.345-08	1.627-08	3.780-09	8.651-08	2.271-08	5.074-08	8.162-09	3.780-09	8.539-08
120	8.002-09	3.113-08	4.536-08	1.400-09	8.589-08	1.596-08	3.287-08	1.837-08	1.400-09	6.860-08
130	3.360-08	1.778-08	1.779-08	1.430-09	7.060-08	1.512-08	1.804-08	1.703-08	1.430-09	5.162-08
140	2.937-08	9.981-09	2.744-08	5.170-10	6.731-08	1.162-08	1.077-08	2.739-08	5.170-10	5.030-08
150	9.598-09	5.282-09	2.512-08	6.080-11	4.006-08	1.164-08	3.380-09	1.061-08	6.080-11	2.569-08
160	6.756-09	1.122-09	1.382-08	1.170-12	2.170-08	5.713-09	6.675-10	1.000-08	1.170-12	1.638-08
170	3.894-09	5.752-12	4.975-09	2.960-15	8.875-09	3.578-09	2.300-12	3.126-09	2.960-15	6.706-09
180	7.433-10	0.000-00	1.455-09	0.000-00	2.198-09	8.879-11	0.000-00	3.160-11	0.000-00	1.204-10
Total	3.203-07	2.650-07	2.443-07	7.135-07	1.543-06	2.602-07	2.844-07	1.705-07	7.135-07	1.429-06

TABLE A7. Exposure Rate Angle Distribution Inside a 80-psf Barrier with a 20-psf Partition

(R/hr per source photon/cm^2-sec)

Polar Angle (deg)	Radiation Component					Radiation Component				
	EDB-IBS	EBS-IDB	EBS-IBS	EDB-IDB	Total	EDB-IBS	EBS-IDB	EBS-IBS	EDB-IDB	Total
	2.5-ft Partition Radius					5.0-ft Partition Radius				
10	2.708-12	0.000-00	3.245-12	0.000-00	5.950-12	0.000-00	0.000-00	2.933-12	0.000-00	2.933-12
20	1.935-10	0.000-00	3.693-11	0.000-00	2.304-10	0.000-00	0.000-00	9.359-09	0.000-00	9.359-09
30	4.947-10	0.000-00	5.536-10	0.000-00	1.047-09	0.000-00	0.000-00	8.229-11	0.000-00	8.229-11
40	0.000-00	0.000-00	6.304-10	0.000-00	6.304-10	1.761-10	0.000-00	1.827-10	0.000-00	3.560-10
50	0.000-00	0.000-00	5.576-09	0.000-00	5.576-09	6.054-10	0.000-00	3.242-09	0.000-00	3.848-09
60	1.044-09	0.000-00	2.191-09	0.000-00	3.236-09	3.028-10	0.000-00	1.850-09	0.000-00	2.153-09
70	1.310-10	0.000-00	6.043-09	0.000-00	6.175-09	9.861-09	0.000-00	2.143-09	0.000-00	1.200-08
80	3.120-08	3.735-08	8.904-09	3.032-08	1.078-07	8.674-09	3.196-08	5.490-09	3.032-08	7.644-08
90	4.893-09	5.667-08	1.115-08	1.868-07	2.595-07	8.288-09	3.459-08	1.101-08	1.868-07	2.407-07
100	3.972-09	2.379-08	4.588-08	4.770-09	7.841-08	1.231-08	4.545-08	5.092-09	4.770-09	6.762-08
110	2.446-10	4.561-08	7.780-09	7.910-10	5.443-08	5.921-09	2.077-08	6.638-09	7.910-10	3.412-08
120	8.435-09	1.202-08	5.945-09	1.930-10	2.659-08	5.041-09	1.625-08	2.176-09	1.930-10	2.366-08
130	2.337-09	1.308-08	4.480-09	1.750-10	2.007-08	5.492-09	1.322-08	1.893-08	1.750-10	3.782-08
140	4.088-09	5.805-09	1.667-08	4.680-11	2.661-08	2.154-09	5.336-09	7.513-09	4.680-11	1.505-08
150	3.691-09	1.477-09	6.310-09	1.890-12	1.148-08	2.884-09	2.420-09	1.202-08	1.890-12	1.733-08
160	1.570-09	3.578-10	4.933-09	8.480-15	6.861-09	1.210-09	3.629-10	5.697-09	8.480-15	7.270-09
170	8.029-10	6.014-13	2.464-09	6.030-18	3.268-09	9.021-10	3.632-13	9.255-10	6.030-18	1.828-09
180	9.629-11	0.000-00	1.874-10	0.000-00	2.837-10	8.673-12	0.000-00	5.738-12	0.000-00	1.441-11
Total	6.320-08	1.961-07	1.297-07	2.231-07	6.122-07	6.385-08	1.704-07	9.235-08	2.231-07	5.497-07

TABLE A8. Exposure Rate Angle Distribution Inside a 20-psf Barrier with a 40-psf Partition

(R/hr per source photon/cm^2-sec)

Polar Angle (deg)	Radiation Component					Radiation Component				
	EDB-IBS	EBS-IDB	EBS-IBS	EDB-IDB	Total	EDB-IBS	EBS-IDB	EBS-IBS	EDB-IDB	Total
	2.5-ft Partition Radius					5.0-ft Partition Radius				
10	0.000-00	0.000-00	0.000-00	0.000-00	0.000-00	0.000-00	0.000-00	0.000-00	0.000-00	0.000-00
20	2.207-15	0.000-00	8.253-10	0.000-00	8.253-10	2.432-09	0.000-00	1.923-11	0.000-00	2.451-09
30	1.976-09	0.000-00	2.932-10	0.000-00	2.269-09	3.564-11	0.000-00	5.362-10	0.000-00	5.719-10
40	1.368-09	0.000-00	2.671-09	0.000-00	4.039-09	7.899-10	0.000-00	1.602-09	0.000-00	2.392-09
50	3.411-09	0.000-00	6.058-09	0.000-00	9.469-09	5.044-09	0.000-00	3.114-09	0.000-00	8.159-09
60	1.959-08	0.000-00	1.024-08	0.000-00	2.983-08	3.160-09	0.000-00	2.599-09	0.000-00	5.760-09
70	4.908-09	0.000-00	5.746-09	0.000-00	1.065-09	5.610-08	0.000-00	1.294-08	0.000-00	6.903-08
80	1.344-07	2.907-08	7.657-09	9.820-08	2.693-07	4.372-08	1.901-08	1.759-08	9.820-08	1.785-07
90	6.239-08	2.377-08	1.121-08	5.895-07	6.869-07	1.079-07	3.153-08	1.527-08	5.895-07	7.442-07
100	4.344-08	3.454-08	2.720-09	1.860-08	9.930-08	7.664-08	3.438-08	1.806-08	1.860-08	1.477-07
110	7.655-08	2.172-08	1.346-08	3.780-09	1.155-07	7.815-08	1.847-08	2.109-08	3.780-09	1.215-07
120	4.768-08	1.258-08	8.755-09	1.400-09	7.042-08	4.177-08	1.445-08	1.017-08	1.400-09	6.779-08
130	4.943-08	5.647-09	2.280-08	1.430-09	7.931-08	3.652-08	5.748-09	1.510-08	1.430-09	5.880-08
140	7.718-08	2.364-09	1.499-08	5.170-10	9.505-08	2.186-08	3.112-09	1.254-08	5.170-10	3.803-08
150	1.057-08	1.210-09	4.244-09	6.080-11	1.608-08	1.581-08	1.166-09	6.211-09	6.080-11	2.325-08
160	1.147-08	1.361-10	9.818-09	1.170-12	2.143-08	1.203-08	1.260-10	5.676-09	1.170-12	1.783-08
170	5.022-09	1.008-13	3.299-09	2.960-15	8.321-09	6.936-09	4.610-14	1.773-09	2.960-15	8.709-09
180	1.440-09	0.000-00	6.148-10	0.000-00	2.055-09	1.982-10	0.000-00	3.833-11	0.000-00	2.365-10
Total	5.509-07	1.310-07	1.254-07	7.135-07	1.521-06	5.091-07	1.279-07	1.443-07	7.135-07	1.495-06

TABLE A9. Exposure Rate Angle Distribution Inside a 40-psf Barrier With a 40-psf Partition

(R/hr per source photon/cm^2-sec)

Polar Angle (deg)	Radiation Component					Radiation Component				
	EDB-IBS	EBS-IDB	EBS-IBS	EDB-IDB	Total	EDB-IBS	EBS-IDB	EBS-IBS	EDB-IDB	Total
	2.5-ft Partition Radius					5.0-ft Partition Radius				
10	0.000-00	0.000-00	1.052-10	0.000-00	1.052-10	0.000-00	0.000-00	1.677-12	0.000-00	1.677-12
20	0.000-00	0.000-00	3.303-11	0.000-00	3.303-11	0.000-00	0.000-00	4.316-11	0.000-00	4.316-11
30	0.000-00	0.000-00	1.010-10	0.000-00	1.010-10	1.317-09	0.000-00	1.337-09	0.000-00	2.655-09
40	0.000-00	0.000-00	2.443-09	0.000-00	2.443-09	6.080-11	0.000-00	6.663-10	0.000-00	7.273-10
50	2.318-09	0.000-00	3.296-09	0.000-00	5.614-09	1.646-09	0.000-00	1.018-09	0.000-00	2.665-09
60	5.691-08	0.000-00	7.343-09	0.000-00	6.425-08	1.790-09	0.000-00	1.900-09	0.000-00	3.690-09
70	4.290-09	0.000-00	7.469-08	0.000-00	7.898-08	3.111-08	0.000-00	2.681-08	0.000-00	5.793-08
80	4.376-12	2.049-08	1.457-08	5.557-08	9.063-08	4.782-08	2.808-08	5.489-09	5.557-08	1.369-07
90	2.923-08	3.281-08	4.564-09	3.375-07	4.041-07	3.235-08	4.385-08	1.115-08	3.375-07	4.249-07
100	4.423-09	3.171-08	2.601-08	9.370-09	7.151-08	5.119-08	4.017-08	3.513-08	9.370-09	1.359-07
110	4.346-08	2.577-08	2.885-08	1.710-09	9.979-08	7.189-08	2.328-08	3.618-08	1.710-09	1.331-07
120	5.818-08	1.234-08	4.496-09	5.140-10	7.553-08	2.232-08	1.109-08	3.854-08	5.140-10	7.246-08
130	1.514-08	7.497-09	3.339-08	4.950-10	5.652-08	2.462-08	5.310-09	2.333-08	4.950-10	5.376-08
140	1.966-08	3.350-09	2.124-08	1.530-10	4.440-08	8.827-09	2.015-09	8.075-09	1.530-10	1.907-08
150	1.095-08	9.976-10	9.435-09	1.050-11	2.139-08	4.771-09	8.531-10	1.061-08	1.050-11	1.624-08
160	1.035-08	1.099-10	4.722-09	9.560-14	1.518-08	6.251-09	1.920-10	7.253-09	9.560-14	1.370-08
170	2.242-09	1.812-14	5.378-09	1.290-16	7.620-09	2.619-09	1.506-14	1.811-09	1.290-16	4.430-09
180	8.483-10	0.000-00	9.266-10	0.000-00	1.775-09	3.838-11	0.000-00	9.963-11	0.000-00	1.380-10
Total	2.580-07	1.351-07	2.415-07	4.053-07	1.040-06	3.076-07	1.548-07	2.094-07	4.053-07	1.077-06

TABLE A10. Exposure Rate Angle Distribution Inside a 80-psf Barrier with a 40-psf Partition

(R/hr per source photon/cm^2-sec)

Polar Angle (deg)	Radiation Component					Radiation Component				
	EDB-IBS	EBS-IDB	EBS-IBS	EDB-IDB	Total	EDB-IBS	EBS-IDB	EBS-IBS	EDB-IDB	Total
	2.5-ft Partition Radius					5.0-ft Partition Radius				
10	0.000-00	0.000-00	8.750-13	0.000-00	8.750-13	0.000-00	0.000-00	1.260-13	0.000-00	1.260-13
20	5.305-11	0.000-00	1.000-10	0.000-00	1.531-10	1.030-10	0.000-00	1.826-11	0.000-00	1.212-10
30	8.257-10	0.000-00	2.299-10	0.000-00	1.055-09	1.865-10	0.000-00	4.205-11	0.000-00	2.285-10
40	1.410-10	0.000-00	6.475-10	0.000-00	7.885-10	1.781-11	0.000-00	1.178-12	0.000-00	1.898-11
50	5.410-10	0.000-00	3.284-10	0.000-00	8.690-10	1.870-10	0.000-00	2.572-09	0.000-00	2.759-09
60	2.447-09	0.000-00	1.433-09	0.000-00	3.881-09	2.954-10	0.000-00	8.371-11	0.000-00	3.791-10
70	1.104-08	0.000-00	1.845-09	0.000-00	1.289-08	4.932-09	0.000-00	2.447-09	0.000-00	7.380-09
80	1.383-08	1.323-08	6.436-08	1.686-08	1.083-07	9.029-09	1.300-08	1.639-09	1.686-08	4.064-08
90	3.357-09	1.776-08	1.326-08	1.052-07	1.396-07	9.413-09	1.964-08	1.926-09	1.052-07	1.362-07
100	1.952-08	2.474-08	5.401-09	2.460-09	5.212-08	8.035-09	1.331-08	1.563-08	2.460-09	3.944-08
110	9.078-09	7.991-09	5.838-09	3.700-10	2.328-08	8.053-09	1.355-08	3.161-08	3.700-10	5.358-08
120	8.948-09	5.300-09	1.605-08	7.460-11	3.037-08	1.493-08	7.980-09	1.791-08	7.460-11	4.089-08
130	3.198-09	2.639-09	5.279-09	6.340-11	1.118-08	4.321-09	4.874-09	2.914-09	6.340-11	1.217-08
140	4.245-09	1.751-09	5.214-09	1.450-11	1.122-08	3.880-09	1.961-09	5.420-09	1.450-11	1.128-08
150	3.757-09	5.144-10	6.048-09	3.530-13	1.032-08	3.165-09	8.318-10	3.976-09	3.530-13	7.973-09
160	1.118-09	7.111-11	1.675-09	8.130-16	2.864-09	3.180-09	8.555-11	2.022-09	8.130-16	5.288-09
170	1.284-09	1.555-15	1.307-09	2.920-19	2.591-09	1.277-09	7.032-14	7.054-10	2.920-19	1.982-09
180	1.473-10	0.000-00	3.683-10	0.000-00	5.156-10	1.551-11	0.000-00	3.475-11	0.000-00	5.026-11
Total	8.356-08	7.402-08	1.294-07	1.250-07	4.119-07	7.103-08	7.539-08	8.896-08	1.250-07	3.603-07

APPENDIX B

GRAS1 Monte Carlo Procedure

The GRAS1 Monte Carlo Procedure is a modified version of the GRASS Monte Carlo Procedure.[9] GRASS was written in FORTRAN for an IBM 1130 computer to calculate the barrier-scattered flux energy and exposure angle distribution at a point inside a cylindrical barrier exposed to gamma rays from a plane source. GRASS was written specifically for fallout shielding calculations. A complete description of the procedure along with utilization instructions is given in Reference 9. The GRAS1 procedure is basically the same as GRASS; therefore, only the changes will be described here.

The modifications incorporated in GRAS1 include 1) a generalized cylindrical geometry capability, 2) the separation of the results into components, and 3) biasing techniques to improve the statistical accuracy of the components. These changes were made to make the GRASS procedure applicable to fallout shielding calculations where interior partitions and/or basements are considered.

GRASS has a fixed geometry consisting of a single cylindrical barrier located upright above a plane gamma source. The GRAS1 procedure will accept any geometry made up of material regions which are defined by two types of boundaries: 1) concentric cylinders and 2) planes perpendicular to the centerline of the cylindrical boundaries. The centerline is perpendicular to the source plane. GRAS1 is limited to eight material regions and eight boundaries. The materials are defined by two sets of cross section data and up to five material densities. The mathematical relationships describing the boundaries and regions were taken from the COHORT procedure.[10]

In fallout shielding calculations involving interior partitions, it is instructive to classify the radiation arriving at the detector according to the regions in which scattering occurred. In GRAS1, the results are divided into 3 components defined by the mode of propagation of the gamma rays through the barrier and partition:

1. Gamma rays having the initial collision in a partition (EDB-IBS).
2. Gamma rays having collisions only in the exterior barrier (EBS-IDB).
3. Gamma rays having collisions in both the exterior barrier and the partition (EBS-IBS).

These results are summed to give the total barrier-scattered flux and exposure rate.

The number of gamma-ray collisions occurring in a partition that is located within a somewhat thicker barrier may be very small compared to the number of collisions occurring in the barrier. If similar statistical accuracy is to be obtained for each component, approximately the same number of collisions should occur in both the barrier and the partition. Therefore, special biasing was incorporated to improve the statistical accuracy of the EDB-IBS and EBS-IBS components. A different type of biasing was used for each component.

To improve the statistical accuracy of the EDB-IBS component, it is necessary to increase the number of gamma rays passing directly through the exterior barrier. This is done by using the exponential transformation to increase the mean free path of the gamma rays before the first collision. The exponential transformation is well known and has frequently been used in shielding calculations involving shields several mean-free paths in thickness.

In brief, a pseudo total macroscopic cross section is computed using the equation

$$\overline{\Sigma_T}(E) = \Sigma_T(E)[1-ET]$$

where $\Sigma_T(E)$ is the total macroscopic cross section for the exterior barrier

at energy E, and ET is an input parameter <1.0. This pseudo cross section is then used instead of $\Sigma_T(E)$ to compute the random path length to the first collision.

The biasing introduced in the gamma-ray weight is removed by adjusting the weight of the gamma ray. If the gamma ray has its initial collision in the exterior barrier, the new gamma-ray weight is given by the equation

$$W' = W \frac{\Sigma_T(E)}{\overline{\Sigma}_T(E)} e^{-D[\Sigma_T(E)-\overline{\Sigma}_T(E)]}$$

where W is the original weight and D is the distance to the collision point. If the gamma ray passes through the exterior barrier before having a collision, the weight is given by the equation

$$W' = We^{-S[\Sigma_T(E)-\overline{\Sigma}_T(E)]}$$

where S is the path length of the gamma ray through the exterior barrier.

The exponential transformation is applied to a fraction of the source gamma rays which are selected at random. This fraction is an input parameter. Biasing is applied only to gamma rays that would intersect an inside partition if the random path length selected were large enough.

To improve the statistical accuracy of the EBS-IBS component, the number of gamma rays that have a collision in the barrier and go to the partition before undergoing the next collision must be increased. This is done by splitting a fraction of the gamma rays which have collisions in the barrier into two gamma rays. This fraction is an input parameter in the program, and the gamma rays to be split are selected at random. Trial scattering angles for one of the two gamma rays are selected from the Klein-Nishina formula until an angle is selected such that the gamma ray projected through this angle will intersect the partition. Knowing the gamma ray will hit the partition, it is forced to scatter at the selected

angle, directly to the partition. At the position on the partition surface where the gamma enters, a sub-history is formed and the gamma ray is traced until it is killed. Sub-histories are killed by the same procedures as the original histories.

The weight of the sub-history is calculated from the equation

$$W' = \frac{W}{N} e^{-\rho}$$

where W is the weight of the original particle,

N is the number of scattering angles selected before a successful angle was calculated, and

ρ is the number of mean free paths between the collision point and the inside partition.

The original gamma-ray history continues at the end of the sub-history. Its new weight is

$$W'' = W - \frac{W}{N} .$$

UNCLASSIFIED
Security Classification

DOCUMENT CONTROL DATA - R & D

(Security classification of title, body of abstract and indexing annotation must be entered when the overall report is classified)

1. ORIGINATING ACTIVITY (Corporate author)	2a. REPORT SECURITY CLASSIFICATION
Radiation Research Associates, Inc. 3550 Hulen Street Fort Worth, Texas 76107	UNCLASSIFIED
	2b. GROUP

3. REPORT TITLE

Monte Carlo Study of Interior Partition Effects on Fallout Shielding

4. DESCRIPTIVE NOTES (Type of report and inclusive dates)

Final Report

5. AUTHOR(S) (First name, middle initial, last name)

J. H. Price
R. L. French

6. REPORT DATE	7a. TOTAL NO. OF PAGES	7b. NO. OF REFS
15 January 1969	51	13

8a. CONTRACT OR GRANT NO.	9a. ORIGINATOR'S REPORT NUMBER(S)
N0022868C1770	
b. PROJECT NO. OCD Work Unit No. 1112H	RRA-T91
c.	9b. OTHER REPORT NO(S) (Any other numbers that may be assigned this report)
d.	NRDL TRC-69-5

10. DISTRIBUTION STATEMENT

This document has been approved for public release and sale; its distribution is unlimited.

11. SUPPLEMENTARY NOTES	12. SPONSORING MILITARY ACTIVITY
Work performed for OCD through the U.S. Naval Radiological Defense Laboratory, San Francisco, California 94135	Office of Civil Defense Office of the Secretary of the Army Washington, D.C. 20310

13. ABSTRACT

Protection factors were calculated by Monte Carlo for cylindrical barriers with a concentric interior partition. The barrier thicknesses were 20, 40, and 80 psf and the partition thicknesses were 20 and 40 psf. The radius of the barrier was 10.0 ft and the interior partition had radii of 2.5, 5.0 and 10.0 ft. The cylindrical concrete barriers were infinite in height. The source was an infinite plane ^{60}Co source which was assumed to represent fallout. The Engineering Method was also used to calculate protection factors for the cylindrical barriers, and the results were compared with the Monte Carlo data.

The Monte Carlo protection factors showed no consistent dependence upon the radius of the partition. The 40-psf partition was found to increase the protection factors of the barriers by as much as a factor of 2.47. The increases in the protection factors due to the 40-psf partition were all the same within 26 percent for the different partition radii and barrier thicknesses. The Monte Carlo and Engineering Method protection factors had an average difference of 7.7 percent with the largest difference being 22 percent. The Engineering Method results were consistently higher. Interior partition reduction factors were calculated from the Monte Carlo data. These factors were found to be as much as 25 percent higher than similar Engineering Method reduction factors. Use of these reduction factors in the Engineering Method gave protection factors which agreed much better with the Monte Carlo protection factors.

DD FORM 1 NOV 65 1473 REPLACES DD FORM 1473, 1 JAN 64, WHICH IS OBSOLETE FOR ARMY USE.

UNCLASSIFIED
Security Classification

14. KEY WORDS	LINK A		LINK B		LINK C	
	ROLE	WT	ROLE	WT	ROLE	WT
Protection Factor						
Fallout Shielding						
Interior Partition Effects						
Engineering Method						
Monte Carlo Calculations						
Cobalt-60						